Induction of human trophoblast stem cells from somatic cells and pluripotent stem cells

Gaël Castel, Dimitri Meistermann, Betty Bretin, Julie Firmin, Justine Blin, Sophie Loubersac, Alexandre Bruneau, Simon Chevolleau, Stéphanie Kilens, Caroline Chariau, et al.

Cell Reports

Article

Induction of Human Trophoblast Stem Cells from Somatic Cells and Pluripotent Stem Cells

Graphical Abstract

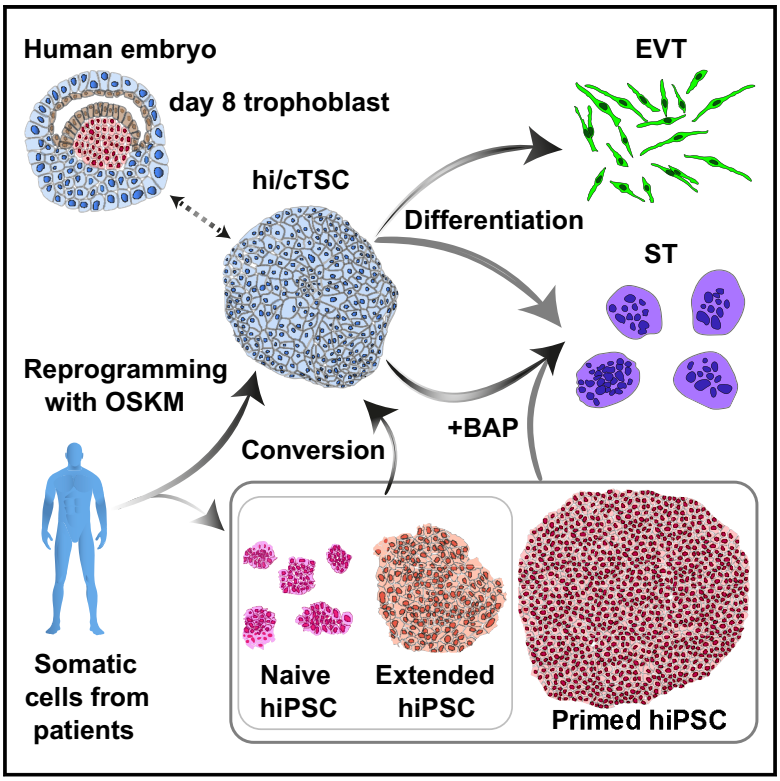

Highlights

- Reprogramming of patient somatic cells to induced hTSCs with OSKM
- Conversion of naive and extended hPSCs to hTSCs
- Comparison of models of the human trophoblast lineage
- h(i/c)TSCs are akin to day 8 trophoblasts of the human embryo

Authors

Gaël Castel, Dimitri Meistermann, Betty Bretin, ..., Hiroaki Okae, Thomas Fréour, Laurent David

Correspondence

laurent.david@univ-nantes.fr

In Brief

Castel et al. report the generation of patient-specific human induced trophoblast stem cells via two methods: (1) somatic cell reprogramming with OSKM and (2) conversion of naive and extended hiPSCs. Their findings open avenues to study placental diseases and relations between the trophoblast lineage, pluripotency, and the human embryo.

Castel et al., 2020, Cell Reports *33*, 108419
November 24, 2020
https://doi.org/10.1016/j.celrep.2020.108419

CellPress

Cell Reports

CellPress
OPEN ACCESS

Article

Induction of Human Trophoblast Stem Cells from Somatic Cells and Pluripotent Stem Cells

Gaël Castel,[1] Dimitri Meistermann,[1,2] Betty Bretin,[1] Julie Firmin,[1,3] Justine Blin,[4] Sophie Loubersac,[3] Alexandre Bruneau,[1] Simon Chevolleau,[1] Stéphanie Kilens,[1] Caroline Chariau,[5] Anne Gaignerie,[5] Quentin Francheteau,[5] Harunobu Kagawa,[6] Eric Charpentier,[5] Léa Flippe,[1] Valentin François--Campion,[1] Sandra Haider,[7] Bianca Dietrich,[7] Martin Knöfler,[7] Takahiro Arima,[8] Jérémie Bourdon,[2] Nicolas Rivron,[6] Damien Masson,[4,9] Thierry Fournier,[10] Hiroaki Okae,[8] Thomas Fréour,[1,3] and Laurent David[1,5,11,*]

[1]Université de Nantes, CHU Nantes, INSERM, Centre de Recherche en Transplantation et Immunologie, UMR 1064, ITUN, 44000 Nantes, France
[2]LS2N, Université de Nantes, CNRS, Nantes, France
[3]Service de Biologie de la Reproduction, CHU Nantes, Nantes, France
[4]CHU Nantes, Laboratory of Clinical Biochemistry, Nantes, France
[5]Université de Nantes, CHU Nantes, SFR Santé, FED 4203, INSERM UMS 016, CNRS UMS 3556, Nantes, France
[6]Institute of Molecular Biotechnology, Austrian Academy of Science, Vienna, Austria
[7]Department of Obstetrics and Gynaecology, Medical University of Vienna, Reproductive Biology Unit, Währinger Gürtel 18-20, 5Q, 1090 Vienna, Austria
[8]Department of Informative Genetics, Environment and Genome Research Center, Tohoku University Graduate School of Medicine, Sendai 980-8575, Japan
[9]Université de Nantes, INSERM, U1235, Nantes, France
[10]Université de Paris, INSERM, UMR-S 1139, 3PHM, 75006 Paris, France
[11]Lead Contact
*Correspondence: laurent.david@univ-nantes.fr
https://doi.org/10.1016/j.celrep.2020.108419

SUMMARY

Human trophoblast stem cells (hTSCs) derived from blastocysts and first-trimester cytotrophoblasts offer an unprecedented opportunity to study the placenta. However, access to human embryos and first-trimester placentas is limited, thus preventing the establishment of hTSCs from diverse genetic backgrounds associated with placental disorders. Here, we show that hTSCs can be generated from numerous genetic backgrounds using post-natal cells via two alternative methods: (1) somatic cell reprogramming of adult fibroblasts with OCT4, SOX2, KLF4, MYC (OSKM) and (2) cell fate conversion of naive and extended pluripotent stem cells. The resulting induced/converted hTSCs recapitulated hallmarks of hTSCs including long-term self-renewal, expression of specific transcription factors, transcriptomic signature, and the potential to differentiate into syncytiotrophoblast and extravillous trophoblast cells. We also clarified the developmental stage of hTSCs and show that these cells resemble day 8 cytotrophoblasts. Altogether, hTSC lines of diverse genetic origins open the possibility to model both placental development and diseases in a dish.

INTRODUCTION

During the first trimester of pregnancy, a subset of proliferative villous cytotrophoblasts (VCTs) ensures the development and homeostasis of the placenta. These cells self-renew and differentiate into all cell types of the trophoblast lineage. Therefore, they are considered to be human trophoblast stem cells (hTSCs).

Isolation of hTSCs has been a major issue in the fields of developmental biology and stem cell research. Mouse TSCs were derived in 1998, but hTSCs were isolated only recently (Okae et al., 2018), due to the difficulty to identify the compartment of these cells *in vivo* and the signaling pathways governing their self-renewal. Okae et al. (2018) successfully derived hTSCs from blastocysts and first-trimester VCTs. They designed a medium containing notably epidermal growth factor (EGF), NODAL/transforming growth factor β (TGF-β) pathway inhibitors, and a WNT pathway activator, which allowed prolonged culture of hTSCs. Herein, this medium is referred to as hTSC medium.

hTSCs cultured *in vitro* represent a pristine model to investigate the development of the trophoblast lineage. These cells generate all differentiated trophoblast cell types, comprising the syncytiotrophoblast (ST) and extravillous trophoblasts (EVTs) (Okae et al., 2018). The ST is the multinucleated outer layer of the trophoblast epithelium formed by cell-cell fusion of cytotrophoblasts. The unique structure of the ST facilitates diffusion of nutrients and gases between maternal blood and the fetus and protects the latter from pathogen entry. EVTs are migratory cells formed by epithelial-mesenchymal-like transition of cytotrophoblasts. EVTs invade the decidual stroma, remodel the spiral arteries, and participate to immune tolerance between

the developing conceptus and the mother through a unique pattern of histocompatibility leukocyte antigen (HLA) expression, notably HLA-G (Knöfler et al., 2019; Turco and Moffett, 2019).

hTSCs at the origin of these processes play a central role in the formation of the maternal-fetal interface, and abnormal hTSCs are likely to have dramatic consequences on placental development. This, in turn, can have post-natal outcomes and ultimately provoke chronic disease in the adulthood (Burton et al., 2016). However, we neither understand the nature and incidence of hTSC disorders nor the connection of hTSCs with placental diseases such as preeclampsia, fetal growth restriction, miscarriage, or choriocarcinomas. For this purpose, researchers need to access hTSCs of diverse genetic backgrounds associated with normal and pathological situations. So far, only a few hTSC lines have been isolated from surplus embryos donated to research and from aborted placentas, and we cannot access hTSCs from individuals who were born after placental complications (Ezashi et al., 2019). To overcome these issues, we need alternative methods to generate hTSCs from more accessible sources of cells.

Human induced pluripotent stem cells (hiPSCs), generated by somatic cell reprogramming, have the potential to differentiate into any cell type in the body and give access to patient-specific cells (Kilens et al., 2018; Takahashi et al., 2007). Cell fate conversion is another method to generate cell types of interest, representing a faster approach that does not involve generation of iPSC lines. Chemical compounds can be sufficient to achieve cell fate conversion, which avoids transduction of exogenous factors (Kim et al., 2020). We hypothesized that these reprogramming strategies, largely applied to embryonic lineages, could also give access to extraembryonic cells, including those of the placenta. It has been reported that primed hPSCs, corresponding to the post-implantation epiblast (EPI), acquire a trophoblast-like fate in response to BMP4, A83-01 (NODAL/TGF-β pathway inhibitor), and PD173074 (fibroblast growth factor [FGF] pathway inhibitor), known as BAP treatment (Amita et al., 2013). However, these cells share features with differentiated trophoblasts and do not self-renew, which limits their use to model the human placenta. Also, the BAP model is debated, as some claim that it produces mesoderm, but others amnion-like cells (Bernardo et al., 2011; Guo et al., 2020).

In this study, we applied OCT4, SOX2, KLF4, MYC (OSKM) reprogramming of somatic cells and conversion of pluripotent stem cells to generate human induced and converted TSCs (hiTSCs and hcTSCs, respectively), from patients with diverse genetic backgrounds. Comparison with isogenic hiPSCs, placental cell types (VCTs, VCT-ST cells, EVTs), and previously established hTSC lines confirmed that hi/cTSCs share similar differentiation potential and molecular signature with embryo- and placenta-derived hTSCs. This study paves the way to the production of patient-specific hiTSCs, with applications to obstetric medicine and the treatment of placental diseases.

RESULTS

Somatic Cell Reprogramming into hiTSCs

We recently achieved reprogramming of somatic cells with OSKM into induced naive hPSCs (hiNPSCs), the counterpart of the pre-implantation EPI in human (Kilens et al., 2018). At low passage in t2iLGö medium, in cells that were still expressing OSKM transgenes, we observed cobblestone-shaped morphology that was reminiscent of hTSCs, in accordance with the expression of trophoblast-associated transcription factor *GATA3* (Figures S1A and S1B). This suggested the occurrence of cells with dual potential to become either hTSCs or hiNPSCs, or a heterogeneous cell population. We thus investigated whether specific combinations of OSKM transgenes enabled to enrich the reprogrammed cells with hTSCs. In the majority of cases, cells stopped proliferating at early passages. Only specific stoichiometries yielded naive hPSC (hiNPSCs), but not hTSC lines (5:5:3 and 3:3:3 KOS, K, M multiplicity of infection). These results suggest that the stoichiometry of the OSKM reprogramming factors is not sufficient to reroute OSKM reprogramming toward hTSCs.

We thus hypothesized that the acquisition of the hTSC state might rather reside in environmental cues and repeated OSKM reprogramming in hTSC culture conditions. After 7 days, cells were transferred either in E7 medium that supports the early phase of reprogramming (Chan et al., 2009) or in hTSC medium. After seven additional days, we observed the formation of epithelial colonies in both conditions, although these colonies were more abundant in E7. These results suggest that E7 not only supports the early phase of reprogramming but also promotes a mesenchymal-epithelial transition and the survival of reprogramming intermediates. Clearly, after culture in E7 (from day 7 to 21), cells robustly supported a transition into hTSC medium. Upon additional culture (2 passages), we observed the rapid formation of cobblestone-shaped colonies, morphologically reminiscent of hTSCs (Figure 1A). These cell lines subsequently lost their transgenes (after 10–15 passages) and expressed the *GATA2* and *GATA3* genes associated with the trophoblast lineage (Gerri et al., 2020; Home et al., 2017; Krendl et al., 2017; Meistermann et al., 2019). By contrast, they did not express the pluripotency markers *NANOG* and *KLF17* (data not shown). These cells propagated unlimitedly, showing long-term self-renewal (>70 passages). Based on their morphology, gene expression profile, and culture condition requirement, we referred to these reprogrammed cell lines as hiTSCs (Table S1A).

Cell Fate Conversion of hNPSCs and hEPSs to hTSCs

To further study the plasticity between pluripotent and trophoblast fates, we tested the potential for primed hPSCs that represent the post-implantation EPI (Amit et al., 2000; Thomson et al., 1998), extended hPSCs (hEPSs) that stabilize a high-potency state (Yang et al., 2017), and hNPSCs that reflect the pre-implantation EPI (Guo et al., 2016; Kilens et al., 2018; Takashima et al., 2014) to respond to BAP treatment (Amita et al., 2013). Primed hPSCs were initially cultured in knockout serum replacement (KSR) + FGF2 or iPS-BREW, hEPSs in LCDM, and hNPSCs in t2iLGöY medium. Consistent with previous reports, primed hPSCs rapidly responded to BAP and transdifferentiated into large cell sheets morphologically reminiscent of trophoblasts. Interestingly, BAP culture could also induce similar morphological changes in hNPSCs and hEPSs, although these cell types are reflecting different states of pluripotency (Figure S2A). We confirmed the expression of trophoblast marker genes in all

CellPress
OPEN ACCESS

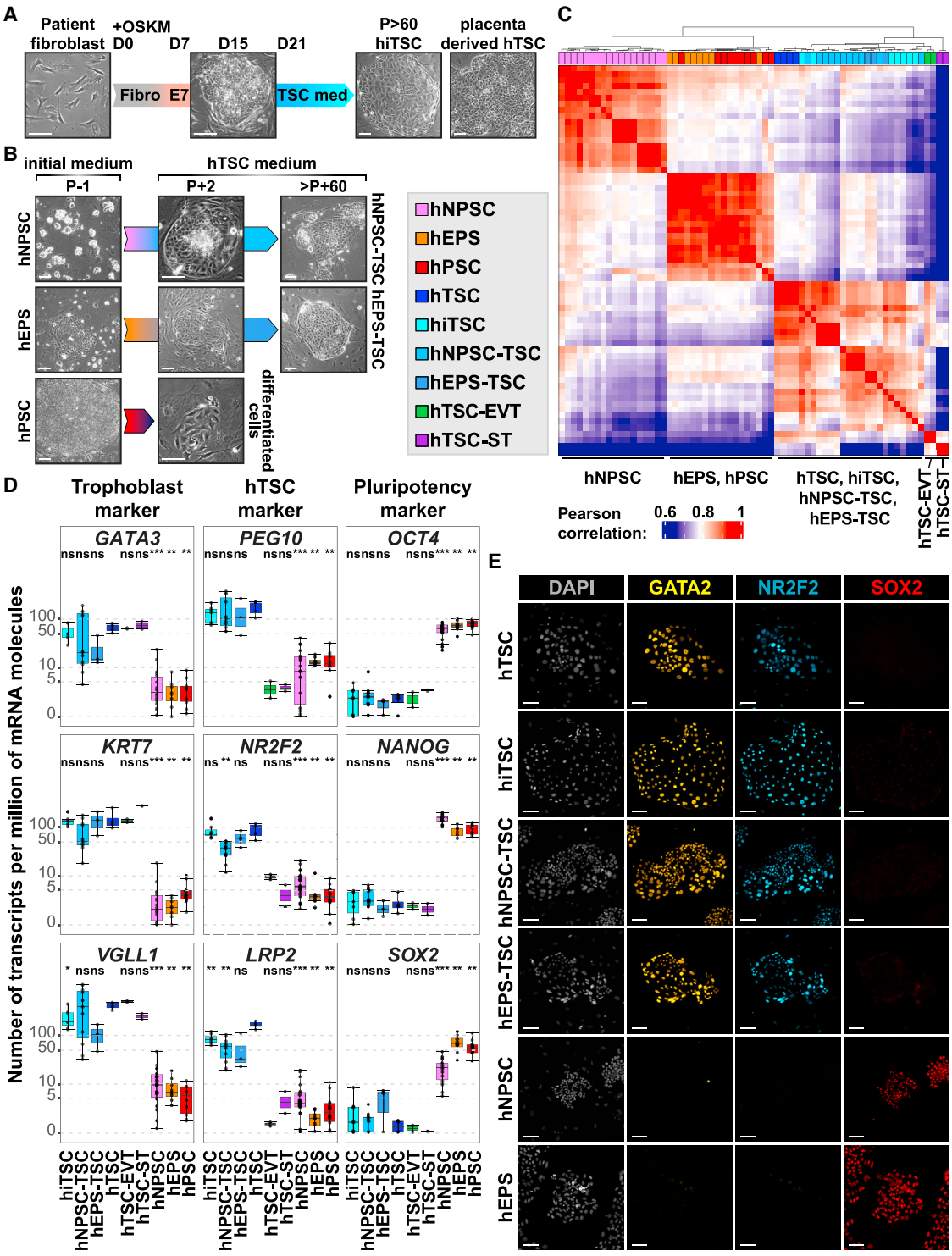

Figure 1. Generation of Human Induced Trophoblast Stem Cells by Reprogramming of Somatic Cells with OSKM and Conversion of Pluripotent Stem Cells

(A) Schematic representation of the reprogramming protocol. Phase contrast pictures show the changes in cell morphology. Placenta-derived hTSCs are shown as controls.

(B) Schematic representation of the conversion protocol. Phase contrast pictures show the changes in cell morphology.

(legend continued on next page)

BAP-treated hPSCs, while we did not detect the expression of genes associated with other lineages, such as mesoderm or amnion (Figures S2B and S2C). These gene expression patterns were comparable to those of hiTSCs treated with BAP, but the cells rapidly stopped proliferating and could not be maintained beyond day 16. We concluded that BAP medium efficiently promoted the conversion of hPSCs to trophoblast-like cells independently from their initial state, but was not suitable for maintenance of self-renewing and expandable hTSCs.

Next, we repeated the similar experiment in hTSC medium. Primed hPSCs did not expand in the hTSC condition, and we observed elevated cell death from 48 to 120 h. Colony integrity faded after 1 or 2 passages and cells stopped proliferating, thus failing to establish hTSCs. Extended hPSCs also experienced an elevated cell death from 48 to 120 h, but few cobblestone-shaped colonies reminiscent of hTSCs emerged after 2 passages (7–14 days) that could be expanded. By sharp contrast, hNPSCs sustained moderate cell death (48–120 h), and numerous colonies similar to hTSCs rapidly emerged (7–14 days) and propagated unlimitedly (>50 passages, Figure 1B). These cells had lost expression of pluripotency markers *NANOG* and *KLF17* and gained expression of trophoblast-associated genes *GATA2* and *GATA3* (data not shown). Hereafter, these cell lines are referred to as hcTSCs (Table S1A).

Molecular Characterization of hiTSCs and hcTSCs

We conducted broad transcriptomic analyses to further characterize hiTSCs and hcTSCs in direct comparison with previously established hTSCs and the differentiated ST cells and EVTs (Okae et al., 2018).

Hierarchical clustering defined three groups of cells: (1) hNPSCs, (2) extended and primed hPSCs, and (3) trophoblasts. Both hiTSCs and hcTSCs clustered together with previously established embryo- and placenta-derived hTSCs to form the group of trophoblasts. This group further subdivided between h(i/c)TSCs, ST cells and EVTs. Pearson correlation analysis further confirmed the proximity of induced, converted, embryo-derived, and placenta-derived hTSCs. Surprisingly, extended and primed hPSCs showed a high degree of transcriptional similarity, despite relative differences in their potential to form hTSCs (Figure 1C). Principal component analysis (PCA) confirmed these observations and produced distinct clusters corresponding to the above-mentioned cell types (Figure S1C). This can suggest that hEPSs might contain rare subpopulations with higher potency comparable to hNPSCs or that the potential to form hTSCs might rely on discrete cellular properties shared between hNPSCs and hEPSs.

Further analysis confirmed that hiTSCs and hcTSCs expressed key trophoblast lineage markers. Notably, the expression levels of *GATA3*, *KRT7*, and *VGLL1* were similar to those found in previously established embryo- and placenta-derived hTSCs (absolute gene expression ranging from 10 to 300 transcripts per million [TPM]). We also identified genes associated with stemness of hTSCs, including *PEG10*, *NR2F2*, and *LRP2*. These were expressed at similar levels in hTSCs, hiTSCs, and hcTSCs, but not in the differentiated ST cells and EVTs (absolute gene expression ranging from 20 to 200 TPM in hTSCs; below 10 TPM in hTSC-ST cells and hTSC-EVTs) (Figure 1D). By contrast, hiTSCs and hcTSCs did not express pluripotency-associated markers such as *NANOG*, *SOX2*, or *OCT4* (*POU5F1*) (absolute gene expression below 10 TPM). We also confirmed that hi/cTSCs did not express genes associated with other lineages (Figure S1D). Globally, gene expression profiles of hi/cTSCs were comparable with those of embryo- and placenta-derived hTSCs, but different from those of hPSCs, which was confirmed by statistical analysis.

We finally analyzed hiTSCs and hcTSCs by immunofluorescence for the trophoblast markers NR2F2 and GATA2 that are expressed in the trophectoderm (TE) of human blastocysts (Meistermann et al., 2019). NR2F2 and GATA2 were highly expressed and localized in nuclei of all cells. Conversely, SOX2 was highly expressed in hPSCs but absent in hTSCs (Figure 1E). These expression patterns were comparable between hiTSCs, hcTSCs, and placenta-derived hTSCs. These results confirm that hi/cTSCs share similar expression profiles with previously established hTSCs.

Functional Validation of hi/cTSCs: Differentiation into EVTs and ST Cells

hTSCs are characterized by their ability to generate highly specialized trophoblast cell types that ensure the unique functions of the placenta. Notably, these cell lineages include the syncytiotrophoblast (ST) and EVTs. Therefore, we assessed the potential for hiTSCs and hcTSCs to differentiate into these cell types, using previously established protocols based on NRG1 for EVT, and forskolin for ST, differentiation (Okae et al., 2018). We directly compared this potential with those of embryo- and placenta-derived hTSCs, along with VCT, ST, and EVT cells isolated from human placentas.

Prior to differentiation assays, hTSCs were cultured either in hypoxia or normoxia to promote EVT or ST formation, respectively (Chng et al., 2010; Wakeland et al., 2017). Initially, we cultured hTSCs on mouse embryonic fibroblast (MEF) feeder

(C) Heatmap of Pearson correlation coefficients of hPSC, hEPS, hNPSC, hiTSC, hcTSC, and hTSC lines along with ST cells and EVTs differentiated from hTSCs. Correlations are determined from the comparison of the 2,770 most over-dispersed genes of the dataset (see STAR Methods). Samples are clustered from the Euclidean distance of correlations, by a hierarchical clustering using Ward's method.

(D) Gene expression levels of indicated lineage markers are shown for hPSC, hEPS, hNPSC, hiTSC, hcTSC, and previously established embryo- and placenta-derived hTSC lines. The differentiated ST cells and EVTs are included as controls. Expression levels are given as number of transcripts per million of mRNA molecules. In each boxplot, the top and bottom of the box represent the third and first quartile, respectively; the band represents the median (second quartile); and error bars show the interquartile range (IQR) (lower bound: Q1 – 1.5 × IQR; upper bound: Q3 + 1.5 × IQR). A Wilcoxon-Mann-Whitney statistical test was performed for each type of hPSC and hTSC, with embryo- and placenta-derived hTSCs taken as the reference group. Asterisks indicate statistical significance of the difference: *p value < 0.05, **p value < 0.01, ***p value < 0.001.

(E) Immunofluorescence images of hTSCs, hiTSCs, hcTSCs, hNPSCs, and hEPSs stained for trophoblast-associated transcription factors GATA2 and NR2F2 and pluripotency-associated transcription factor SOX2. Nuclei were stained with DAPI.

Scale bars, 100 μm.

CellPress
OPEN ACCESS

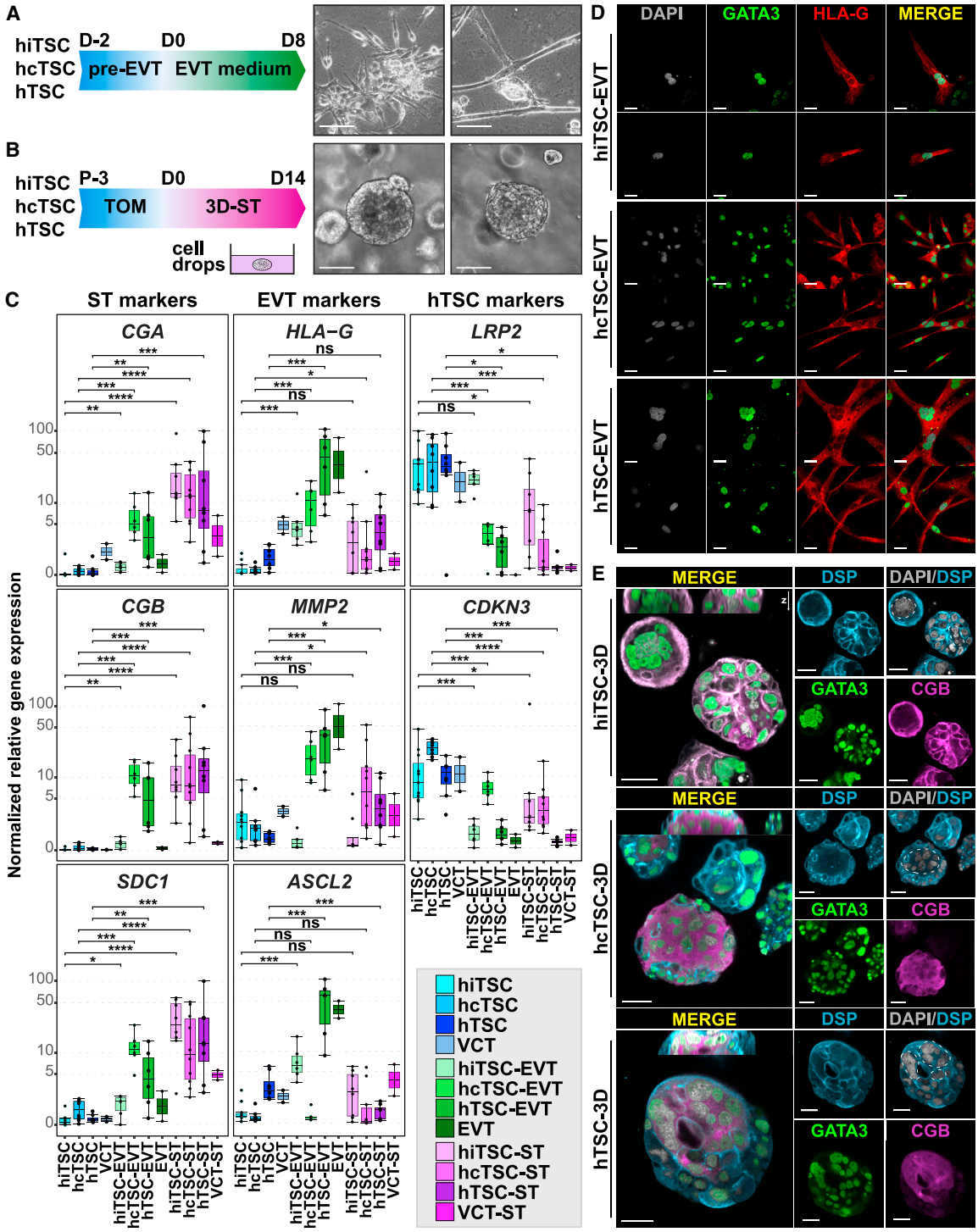

Figure 2. Induced and Converted hTSCs Can Differentiate into Extravillous Trophoblasts and the Syncytiotrophoblast

(A) Schematic representation of the EVT differentiation protocol (left). Bright-field pictures of the EVT progeny of h(i/c)TSCs (right).

(B) Schematic representation of the 3D-ST differentiation protocol (left). Bright-field pictures of the 3D-ST structures derived from h(i/c)TSCs (right).

(C) qRT-PCR quantification of markers associated with ST cells (*CGA*, *CGB*, *SDC1*), EVTs (*HLA-G*, *MMP2*, *ASCL2*), and hTSCs (*LRP2*, *CDKN3*). In each boxplot, the top and bottom of the box represent the third and first quartiles, respectively; the band represents the median (second quartile); and error bars show the IQR (lower bound: Q1 − 1.5 × IQR; upper bound: Q3 + 1.5 × IQR). A Wilcoxon-Mann-Whitney statistical test was performed for each type of hTSC and the differentiated cell progeny. Asterisks indicate statistical significance of the difference: *p value < 0.05, **p value < 0.01, ***p value < 0.001.

(legend continued on next page)

layers that promoted undifferentiated proliferation compared with other matrices. However, we observed that MEFs impaired the formation of ST cells and EVTs so we screened for other matrices to adapt hTSCs prior to differentiation assays. Fibronectin coatings were efficient at maintaining hTSCs over time, and laminin 521 could further enhance proliferation (Figure S3A). For an efficient differentiation, we adjusted the protocols of Okae et al. (2018) as follows: EVT differentiation was enhanced by complementing the medium with IWR-1, which promoted the accumulation of EVT progenitors, as previously described (pre-EVT medium; Haider et al., 2018). For ST and EVT differentiation, we adjusted cell density at seeding from 0.8 to 6.0 × 10^4 cells/cm^2 and the timing of treatment initiation from 0 to 6 h, depending on the lines (Figures 2A and 2B).

Upon optimized ST differentiation, cells upregulated the expression of *CGA*, *CGB*, and *SDC1*, which are not expressed in hTSCs (relative gene expression ranging from 10- to 1,300-fold change). By contrast, *HLA-G*, *MMP2*, and *ASCL2* were globally increased in the EVT differentiation condition (relative gene expression ranging from 10- to 700-fold change). Finally, *LRP2* and *CDKN3* predominantly expressed in hTSCs were downregulated upon differentiation (relative gene expression ranging from 2- to 70-fold change). Importantly, gene expression patterns were comparable with those of placental cells, which was confirmed by statistical analysis (Figure 2C).

Of note, some cell lines did not upregulate *MMP2* upon EVT differentiation, while others did not upregulate *ASCL2*. However, the clear expression of *HLA-G* unequivocally confirmed the EVT identity. This raises the possibility of distinct EVT populations, as previously described (Knöfler et al., 2019; Xiang et al., 2020), or it might reflect intrinsic cellular properties of cell lines. In addition to specific gene expression, EVTs can be reliably identified by dramatic morphological changes resulting in elongated shape (phase contrast images, Figure 2A). Immunostainings for GATA3 and HLA-G confirmed the identity of EVTs differentiated from hiTSCs, hcTSCs, and placenta-derived hTSCs (Figure 2D).

In addition, ST cells can be identified by two important characteristics: the production of human chorionic gonadotropin (hCG) and the fusion of cells that form multinucleated syncytia. After 6 days of forskolin treatment, β-hCG secretion was increased in h(i/c)TSCs, with a mean secretion superior to 3.9 × 10^4 mIU/mL. By contrast, in those conditions, hPSC lines globally did not secrete β-hCG. In line with transcriptomic analysis, both hPSC and hTSC lines secreted β-hCG when treated with BAP (Figure S3D).

Finally, it has been reported that the 3D culture of hTSCs promotes the formation of ST cells (Haider et al., 2018; Okae et al., 2018). Based on trophoblast organoid formation protocols, we embedded hTSCs as single cells in a semi-solid environment made of Matrigel, fibronectin, and laminin 521. Cells were subsequently cultured in human trophoblast organoid medium (TOM) with small modifications (Turco et al., 2018). Within a week, we observed the formation of 3D structures that grew to ~200 μm in diameter after 2 weeks (Figure 2B). These structures contained multinucleated syncytia expressing desmoplakin (DSP) and CGB, and typically containing 6–10 nuclei (Figure 2E). In the majority of cases, fusion of cells occurred in the center of the 3D structures, as previously observed with placenta-derived trophoblast organoids (Haider et al., 2018; Turco et al., 2018). Over time, these placental organoids further grew until they reached confluence within the drops of Matrigel. These larger structures also contained multinucleated ST cells (Figure S3C). Further optimization of culture conditions is needed to determine whether this system will allow expandable culture of hTSC-derived trophoblast organoids. We concluded that optimized differentiation protocols facilitate the formation of functional ST- and EVT-like cells and 3D self-organization from h(i/c)TSC lines. This confirmed the potential for hiTSCs and hcTSCs to form complex placental-like tissues including multiple differentiated and functional cell types.

Dynamics of Cell Fate Conversion from hPSCs into hTSCs

To further understand the conversion process of hPSCs into hTSCs, we projected our cellular models on a PCA, which shows that samples cluster according to their fate. PC1 and PC2 accounted for 18 and 11% of variance, respectively. We identified five main clusters: (1) hNPSCs, (2) hEPSs/hPSCs, (3) hTSCs/hiTSCs/hcTSCs, (4) EVTs, and (5) ST cells (Figure 3A). PC3 accounted for 9% variance and segregated hNPSCs from other cells, thus confirming the particularity of naive pluripotent stem cells, reflecting the early EPI, and capable of efficiently generating hTSCs (Figures 3B and 3C).

We further analyzed the progression of cells during cell fate conversion. All types of hPSCs treated with BAP showed rapid and dramatic transcriptomic changes and became close to differentiated trophoblasts by day 6. Despite some partial overlap with hTSCs, they formed a distinct group, closer to the differentiated EVTs and ST cells. Importantly, hTSCs treated with BAP acquired a similar state, supporting that these transcriptional changes relate to the differentiation of the trophoblast lineage (Figure 3D).

hNPSCs transferred to hTSC medium formed a separate cluster characterized by an intermediate transcriptome (P+2), followed by the acquisition of a hTSC molecular signature (~P+3, Figure 3E). hEPSs had delayed transcriptional variations and remained globally unchanged until day 5 before transiting through an intermediate transcriptional state (P+2), ultimately acquiring a profile characteristic of hTSCs (P+3, Figure 3F). We concluded that hNPSCs and hEPSs transited through an intermediate transcriptional state before ultimately achieving a cell fate conversion into hTSCs. Whether this transcriptional progression reflects a developmental path remains to be investigated (Cinkornpumin et al., 2020). By contrast, primed hPSCs initiated similar transcriptional changes,

(D) Immunofluorescence images of EVTs differentiated from hiTSC, hcTSC, and placenta-derived hTSC lines stained for the trophoblast-associated transcription factor GATA3 and the extravillous trophoblast-specific surface marker HLA-G. Nuclei were stained with DAPI.
(E) Immunofluorescence images of 3D-ST structures derived from hiTSC, hcTSC, and hTSC lines stained for GATA3 and the membrane-associated protein desmoplakin (DSP) highlighting syncytia, along with the syncytiotrophoblast-associated marker CGB. Nuclei were stained with DAPI. Main images correspond to the x-y plane of a single z section. Related orthogonal y-z plane is shown above merged images.
Scale bars: 100 μm in (A) and (B) and 30 μm in (D) and (E).

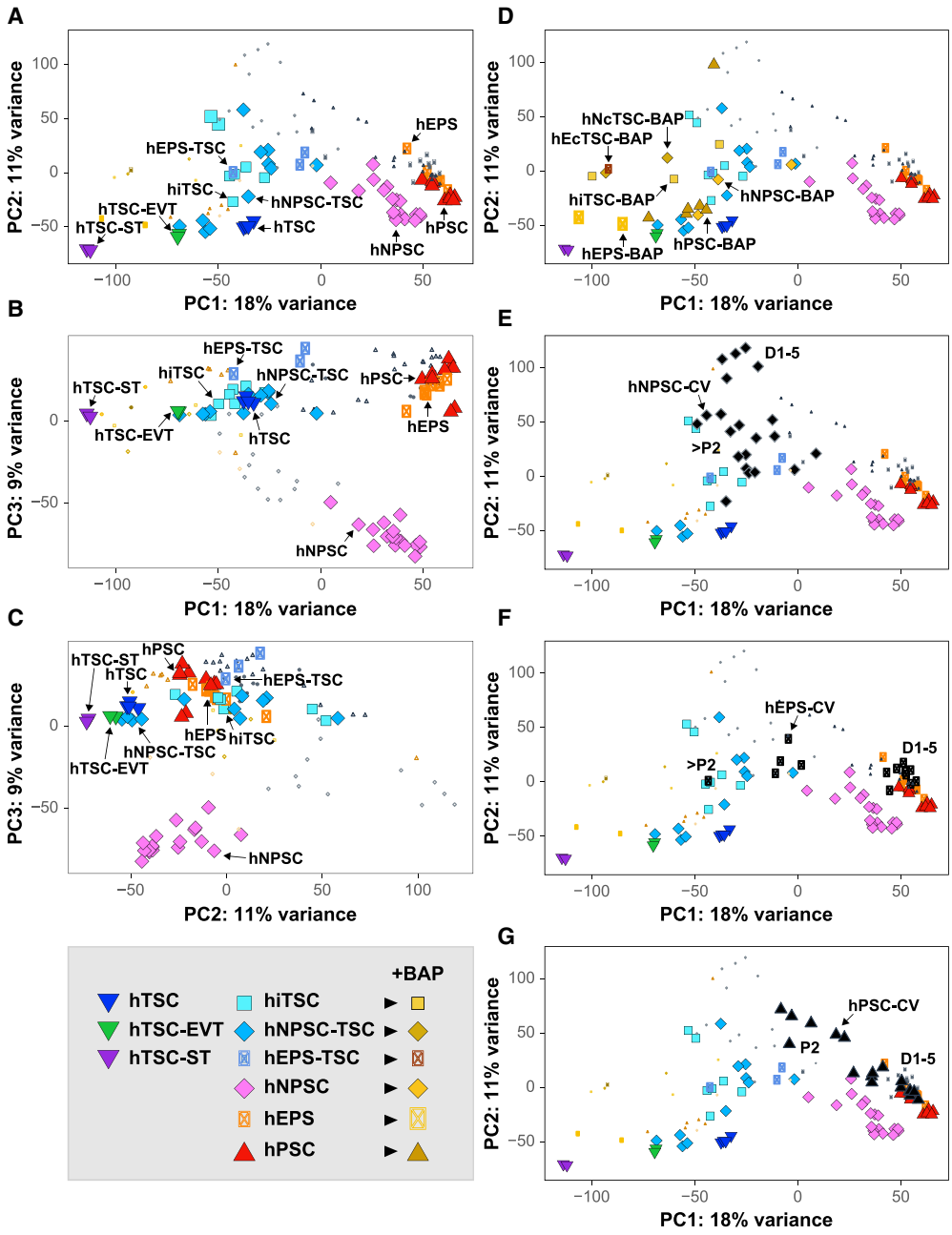

Figure 3. Transcriptional Specificities of h(i/c)TSCs and Intermediate Steps of Cell Fate Conversion

(A–G) PCA analysis of h(i/c)TSCs and hPSCs in maintenance, differentiation, or conversion media. PC1, PC2, and PC3 are displayed for differentiated cells, hPSC and hTSC lines (A–C). PC1 versus PC2 of BAP-treated cells (D), naive hPSCs converted into hTSCs (E), extended hPSCs converted into hTSCs (F) or primed hPSCs treated with hTSC medium (G) are highlighted in specific panels.

but the cell fate conversion was not completed and cells did not acquire hTSC signature (P+2, Figure 3G).

Globally, treatments of hPSCs with either BAP or hTSC medium converged to induce the acquisition of the trophoblast fate, but only hTSC culture condition supported the proliferation and self-renewal programs required to stabilize expandable stem cells. Understanding how external cues are integrated by cells to mediate these different outcomes will allow the identification of determinants of cell fate conversion, self-renewal, and proliferation of the native human placental progenitors.

Modulations of Signaling Pathway Signatures Underly the Conversion of hPSCs to hTSCs

We reasoned that signaling pathway variations upon conversion of hPSCs to hTSCs or differentiated trophoblasts might inform about the mechanisms of specification, self-renewal, and

differentiation of human trophoblast progenitors. We thus performed a clustering analysis to identify co-regulated genes and a pathway enrichment analysis.

Clustering of samples on differentially regulated pathways globally confirmed the sample clustering previously performed on differentially expressed genes. This segregated three main groups: (1) hPSCs, (2) hTSCs, and (3) differentiated trophoblasts. In line with the PCA results, BAP-treated cells (day 6) were akin to ST cells and EVTs and showed profiles of enriched pathways resembling those of differentiated trophoblasts. By contrast, hNPSC-TSCs and hEPS-TSCs shared similar pathway signatures with hiTSCs, embryo-derived, and placenta-derived hTSCs, while primed hPSCs transited in hTSC medium globally failed to acquire hTSC pathway signatures (Figure S4).

The clustering of pathways produced two main groups: (1) pathways associated with hPSCs and (2) pathways associated with trophoblasts. Pathways associated with hPSCs included glycolysis, cell cycle, and base excision repair, in line with previous studies on cell cycle regulation and metabolic state of hPSCs (Kilens et al., 2018). By contrast, hTSCs and differentiated trophoblasts globally shared common pathway signatures, clearly distinct from those of hPSCs.

Differentially regulated pathways included HIPPO, NOTCH, and ERBB pathways, which are main drivers of the self-renewing state of mouse TSCs (El-Hashash et al., 2010; Home et al., 2012; Nishioka et al., 2009; Rayon et al., 2014; Rivron et al., 2018b) and PPARG that is associated with mouse trophoblast proliferation and differentiation (Parast et al., 2009). These results complete previous studies suggesting conserved mechanisms of trophoblast development across mammals (Gerri et al., 2020; Hunkapiller et al., 2011; Saha et al., 2020; Schaiff et al., 2000), while they also highlight specific features of the human trophoblast lineage such as the steroid hormone biosynthesis pathway that was specifically associated with the ST in humans (Malassiné et al., 2003). Moreover, our analysis pointed to additional pathways including MTOR, estrogen, RAP1, and JAK/STAT signaling pathways that seem to be active in h(i/c)TSCs (Figures S4 and S5).

Regarding the MTOR signaling pathway, genes with positive contribution to the eigengene were dominantly expressed in hTSCs. They included *CASTOR1*, an inhibitor of mTORC1, and *PRR5*, a subunit of mTORC2. Also, trophoblast cells downregulated *RRAGD*, an activator of mTORC1. By contrast, hPSCs expressed *MTOR*, *ULK1*, and *SGK1*, which are effectors of mTORC1 signaling. These observations could indicate a switch from TORC1 in hPSCs to TORC2 activity in hTSCs during the cell fate conversion process. Interestingly, we also observed differences in MTOR pathway signatures between the distinct types of hPSCs. Along with other genes, the expression of *DEPTOR*, a regulator of MTOR signaling, was high in hNPSCs, moderate in hEPSs, and low in hPSCs, suggesting a differential regulation of the pathway between these cells associated with different degrees of trophoblast potential (Figure S5).

The estrogen signaling pathway seemed to be active in hTSCs, which is reflecting the response to placental hormones that is observed *in vivo*. This was accompanied with the expression of *CREB3* and *FOS* that can mediate the transcription of estrogen-responsive genes, and the upregulation of keratin genes, such as *KRT17*, *KRT18*, and *KRT19*, in line with the morphological changes associated with the formation of epithelial hTSCs (Figure S5). Conversely to hTSCs, hPSCs expressed *FKBP5* and *HSP90AB1*, which can form a complex that inhibits the translocation of the estrogen receptor to the nucleus (Baker et al., 2018).

hTSCs also expressed *RRAS*, *VAV3*, and *RAC2*, which are effectors of the RAP1 signaling pathway, along with *EGFR* and *GNAI1*, which can signal to RAP1 through receptor tyrosine kinase (RTK)- and G protein-coupled receptor (GPCR)-induced cascades, respectively. By contrast, hEPSs and hPSCs expressed *ID1*, which is inhibited by RAP1, and globally did not express actors of the RAP1 signaling pathway, suggesting that it is not active in these cells. However, hNPSCs expressed *RASGRP2*, which specifically activates RAP1, along with *FGFR3* and *LPAR2*, which encode for two receptors that can signal to RAP1 (Figure S5). These gene expression profiles suggest that the RAP1 signaling pathway might be active in hTSCs and hNPSCs, but is mediated through different input signals, while it is not active in hEPSs and hPSCs.

We also found that hTSCs expressed genes encoding receptors that can activate the JAK/STAT signaling pathway, including *IL10RB*, *CSF3R*, *CSF2RA*, and *IFNGR1*. By contrast, hEPSs and hPSCs expressed *SOCS3*, a member of the suppressor of cytokine signaling protein family that inhibits JAK/STAT signaling, while hNPSCs expressed *SOCS4* and *PTPN2*, which dephosphorylate JAK and STAT proteins thus inhibiting the signaling.

Interestingly, our analysis also pointed to gene expression profiles that suggested crosstalk between the identified pathways. For example, *SFN*, which is associated with cell cycle, was specifically expressed in hTSCs. When bound to KRT17, SFN regulates epithelial cell growth by stimulating the MTOR pathway (Kim et al., 2006). This suggests a potential crosstalk between the cell cycle, estrogen, and MTOR pathways in hTSCs (Figures S4 and S5).

Our analysis highlighted both conserved and divergent expression profiles of signaling pathway components underlying trophoblast specification and self-renewal. hTSC pathway signatures were globally milder than those of differentiated trophoblasts, and the switch between the self-renewing state (hTSC) and the differentiated state (BAP-treated cells) was mainly reflected by an accentuation of these same pathway signatures. This suggests that human trophoblast development is driven by a continuity rather than a sequential switch between different signaling activities and that the strength of the signaling activity correlates with the progression from a self-renewal to a differentiation program. This dampened signaling activity observed in the self-renewing state might reflect the minimal requirement of unspecialized human trophoblast progenitors.

A comprehensive list of pathway components and their contribution to pathway eigengenes can be found in Table S2G. Further knockout experiments are needed to determine how these pathways are modulated between hPSCs, hTSCs, and trophoblast lineages; yet, this analysis gives a global picture of hTSC pathway signatures and changes associated with cell fate conversion of hPSCs.

hTSCs Are Akin to Post-implantation Day 8–10 Cytotrophoblasts

An outstanding question regarding hTSCs is to understand which developmental stage these cells are reflecting. To address

this question, we compared the transcriptomes of hTSCs with single-cell RNA sequencing (scRNA-seq) data of human peri-implantation embryos (146 embryos; 6,838 cells), from day 3 to 14 (prolonged culture of human embryos for 9 days after blastocyst stage) (Petropoulos et al., 2016; Zhou et al., 2019). We projected all cells on a uniform manifold approximation and projection (UMAP) and highlighted sample annotation (Figure 4A, inset). UMAP recapitulated developmental time and fate, showing the succession of eight-cell stage, morula, early blastocyst, EPI, primitive endoderm (PrE), TE, and trophoblast (TB) cells from left to right. We noticed a cluster of trophoblasts with enrichment of apoptosis-related genes that we named "apoptotic trophoblasts" and the previously reported cluster of yolk-sac trophoblasts (Zhou et al., 2019). We further clustered cells on the UMAP, which yielded 19 clusters of cells. In particular, this distinguished clusters associated with the development of the trophoblast lineage: early, medium, and late pre-implantation TE, in line with our recent report (Meistermann et al., 2019); five post-implantation trophoblasts (trophoblast #1 to trophoblast #5); and pre-EVT, EVT, pre-ST, and ST (Figure 4A).

We used gene sets associated with each cluster, or gene sets recently associated with pre-implantation TE, post-implantation trophoblast, EVT, and ST to benchmark the transcriptional signature of h(i/c)TSCs (Xiang et al., 2020) (Figures S6A and S6B). Gene sets specific of each cluster highlighted the hierarchy of transcriptomic changes upon progression toward the trophoblast lineage (Figure S6A). Overall, comparison of transcriptional profiles of h(i/c)TSCs with peri-implantation scRNA-seq datasets pointed that h(i/c)TSCs are related to the trophoblast lineage from day 5 to 12 (Figures S6A and S6B). Curation of the list led us to propose markers of post-implantation trophoblasts that matched hTSC lines and distinguished them from ST cells, EVTs, and hPSC lines (Figure 5). The markers that are better associated with hTSCs are found in the gene sets specific of clusters trophoblast #1 and trophoblast #2, which are mainly composed of cells isolated from day 8 and day 10 embryos. Among those gene lists, we identified markers that have been assessed by immunofluorescence in human embryos: NR2F2, CDX2, GATA3, KRT7, and CCR7 (Deglincerti et al., 2016; Meistermann et al., 2019; Niakan and Eggan, 2013; Petropoulos et al., 2016). Projection of the expression of those markers on the UMAP led us to propose that hTSCs expressed genes associated with clusters trophoblast #1 and trophoblast #2. Indeed, hTSCs are expressing LRP2 and NR2F2, but not CDX2 (marker of medium TE) or EVT or ST markers (Figures 4B and 5). To further support our conclusion, we represented gene set expression across embryonic cell populations and stem cells as violin plots summarizing the heatmap (Figure 6). This representation allows to appreciate genes sets present or absent in each cell type. For example, hNPSCs are displaying high expression of EPI genes, moderate expression of early TE genes, and low expression of post-implantation trophoblast genes. hNPSCs are therefore the closest to EPI. h(i/c)TSCs were akin to the trophoblast #1 and trophoblast #2 clusters, while BAP-treated cells were closer to the trophoblast #5 and pre-ST clusters. Finally, ST and EVT cells derived from hTSC differentiation *in vitro* shared similar expression profiles with those of ST and EVT cells found in the embryo (Figure 6).

Altogether, our analysis points out markers that can distinguish developmental timing of TE and trophoblast cells and associate hTSCs with day 8–10 of development. Those markers notably include LRP2 and NR2F2.

DISCUSSION

In the present study, we generated hiTSCs from patients with diverse genetic backgrounds. We found that the OSKM system was not restricted to embryonic lineages, but was permissive to the trophoblast fate. Therefore, this system, largely accessible to researchers, is suitable for the parallel generation of isogenic hiTSCs and hiPSCs, which could greatly benefit the study of placental diseases. Comparison with primary placental cells and hTSC lines confirmed that hi/cTSCs were similar to embryo- and placenta-derived hTSCs. They recapitulated transcriptome, protein markers, and differentiation potential into EVT and ST cells.

In this study, we also revisited the relations between hPSCs and the trophoblast lineage. We used two different systems to evaluate the potential of hPSCs to generate hTSCs: BAP treatment and transition into hTSC medium. We assessed a broad spectrum of hPSCs, comprising hNPSCs, related to pre-implantation EPI; hEPSs, showing contribution to extra-embryonic lineages in chimeras; and primed hPSCs, related to post-implantation EPI. We found that all types of hPSCs produced differentiated trophoblasts, but not hTSCs, in response to BAP. By contrast, hNPSCs and extended hPSCs, but not primed hPSCs, converted to hTSCs, following transition into hTSC medium.

During the preparation and revision of this manuscript, other groups have reported conflicting evidence that the potential to generate trophoblasts is either higher in ground state or in expanded potential stem cells (Cinkornpumin et al., 2020; Dong et al., 2020; Gao et al., 2019). For example, Gao et al. (2019) claimed that expanded potential hPSCs (hEPSCs), but not hNPSCs (cultured in 5iLAF), can generate hTSCs. Dong et al. (2020) and Cinkornpumin et al. (2020) reported conversion from 5iLAF naive cells. Here, we report successful conversion into hTSCs from the two other main culture media used for hNPSCs (Takashima et al., 2014) and extended hPSCs (Yang et al., 2017). Our results indicate that the potential to engage the trophoblast lineage is common to all hPSCs. However, in our model, only hNPSCs and hEPSs completed cell fate conversion to hTSCs. We concluded that the potential to form hTSCs correlates with the proposed developmental time equivalent of the initial culture, with hNPSCs being the most potent state to form hTSCs. We do not exclude that primed hPSCs could generate hTSCs in another system, but this might rely on other pathways. Further investigations are needed to determine whether plasticity exists in the embryo, between the EPI and the TE, and how it is regulated upon developmental progression.

Another key point of this study was to determine the developmental counterpart of hTSCs in the embryo. To address this, we took advantage of scRNA-seq datasets of the human embryo during the peri-implantation development, from day 3 to 14. Our analysis revealed high complexity of the trophoblast lineage, divided in twelve clusters of cells, including TE, CTB, ST, and EVT. We compared molecular signatures and found that hTSCs resemble NR2F2+ day 8–10 CTB, which is clearly distinct from

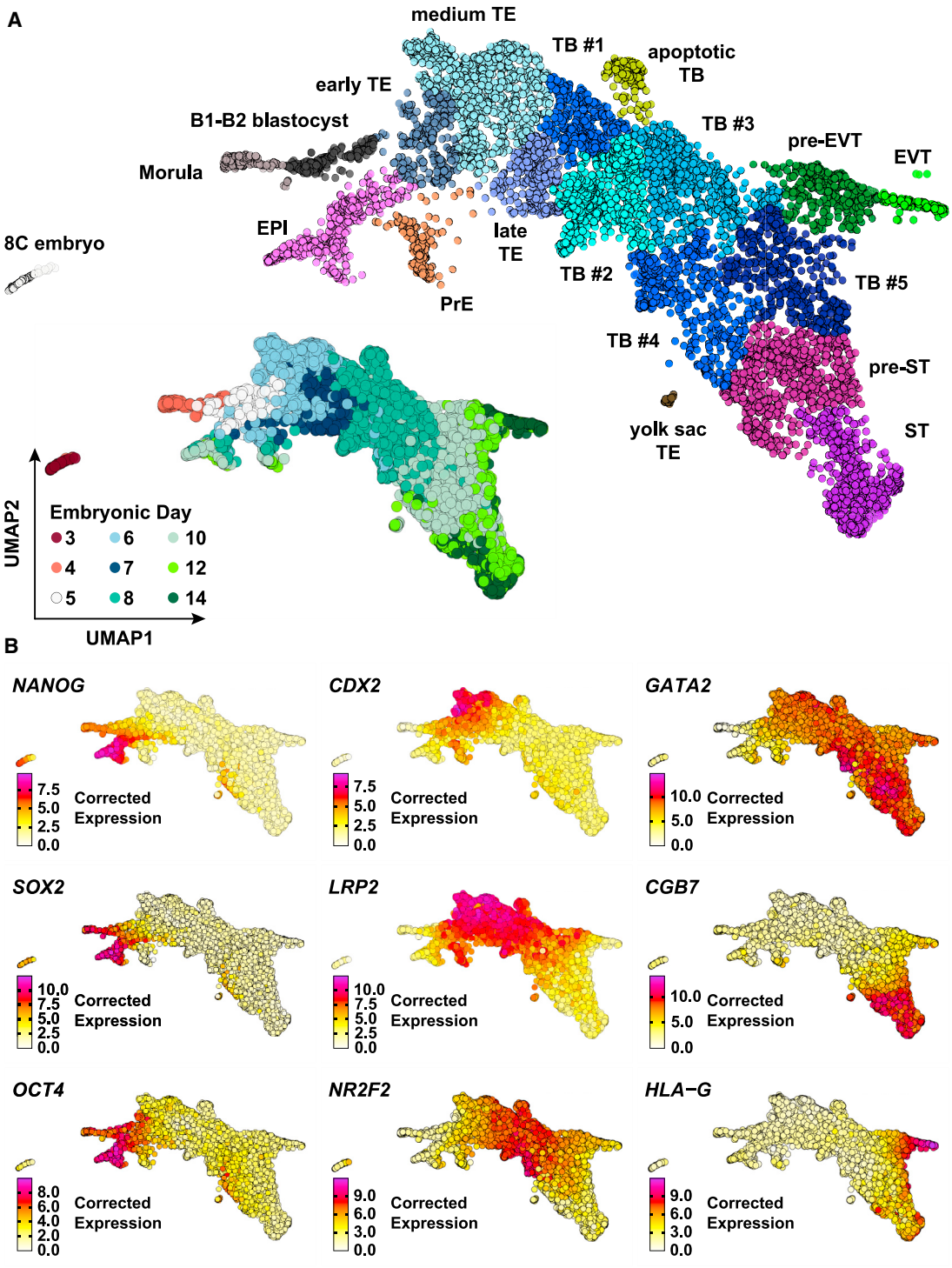

Figure 4. Transcriptomic Analysis of Human Development from Day 3 to 14

(A) UMAP representation of the combined scRNA-seq dataset from Petropoulos et al. (2016) and Zhou et al., (2019), covering eight-cell stage to "day 14" of human development. Cluster analysis revealed 19 clusters, indicated on the UMAP.

(B) Projection of the developmental day annotation on the UMAP.

(C) Projection of expression levels for selected genes on the UMAP. The scale of expression is logarithmic and is equivalent to *a log2*$(x+1)$ transformation of expression counts.

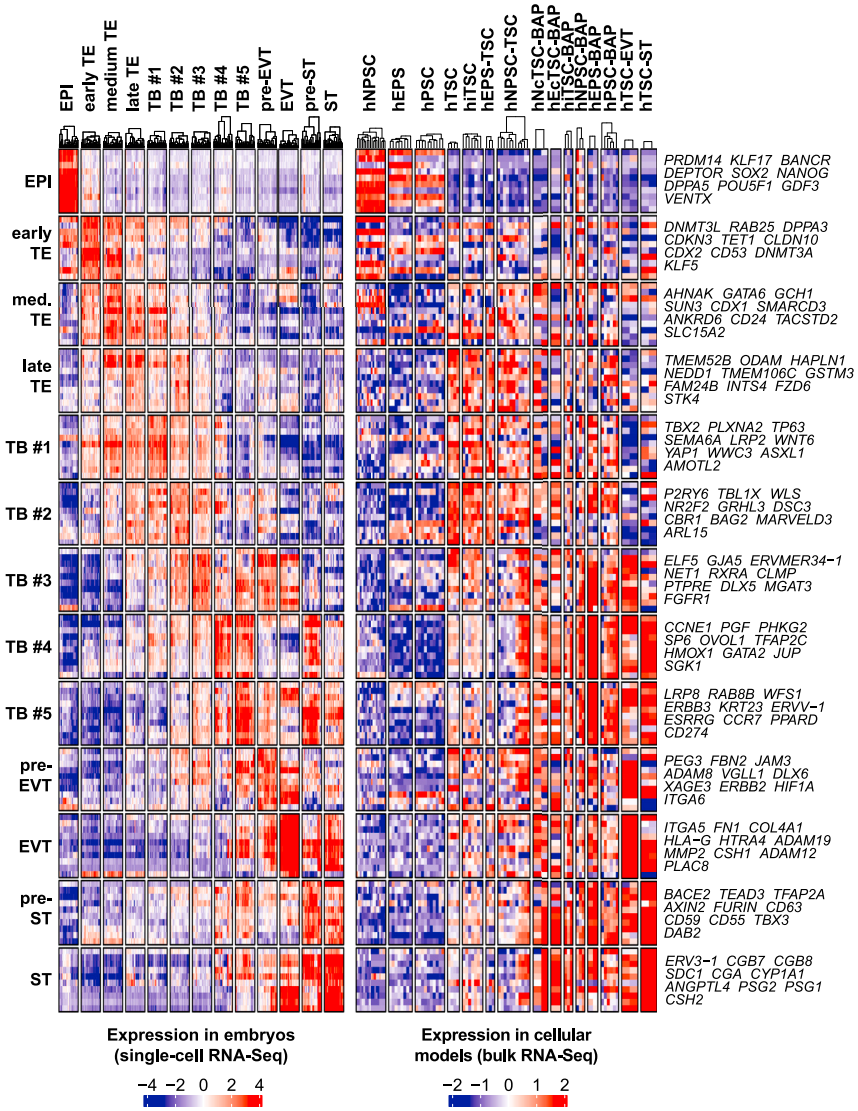

Figure 5. Developmental Matching of hTSCs with Peri-implantation Trophoblasts of the Human Embryo

Gene expression heatmaps of selected markers characterizing embryo cell clusters are shown for scRNA-seq embryo samples (left) or digital gene expression sequencing (DGE-seq) cellular model samples sequenced for this study (right). Expression is *Z* scored. A panel of 10 genes was selected among the best markers of each cell cluster, indicated at the right of the heatmaps. The entire list of markers is available in Table S2. On the left heatmap, 30 cells were randomly selected for each single-cell cluster.

CDX2+ day 5–6 TE. Therefore, hTSCs might be suitable to study early events of trophoblast lineage development, but maybe not for pre-implantation TE. To address this, we need to optimize culture conditions to isolate and maintain human trophectoderm stem cells (hTESCs). Recent studies suggest that this state exists in human, and CDX2+ hTSCs have been obtained, but these cells have not been compared with the human TE yet (Knöfler et al., 2019; Mischler et al., 2019).

Finally, generation of hiTSCs by reprogramming provides a welcome alternative to the derivation of hTSCs from embryos and placentas. This will enlarge the genetic repertoire of hTSC lines and give access to specific genetic backgrounds of interest. A next step is to generate hiTSCs from patients affected by placental disorders. With this strategy, we can now consider studies to investigate the role of genetics in placental development and diseases such as preeclampsia, intrauterine growth restriction, miscarriage, or choriocarcinomas. hiTSCs could also serve for screening new formulations of human embryo culture media, with potential applications to *in vitro* fertilization. New models of the embryo, such as blastoids, could benefit to this field of research (Rivron et al., 2018a). In this context, parallel derivation of isogenic hiTSCs and hiPSCs could provide a valuable source of cells. Overall, the assets of hiTSCs are comparable to the advantages of hiPSCs over hESCs in the field of human development and disease modeling.

STAR★METHODS

Detailed methods are provided in the online version of this paper and include the following:

- KEY RESOURCES TABLE
- RESOURCE AVAILABILITY
  - Lead Contact
  - Materials Availability
  - Data and Code Availability

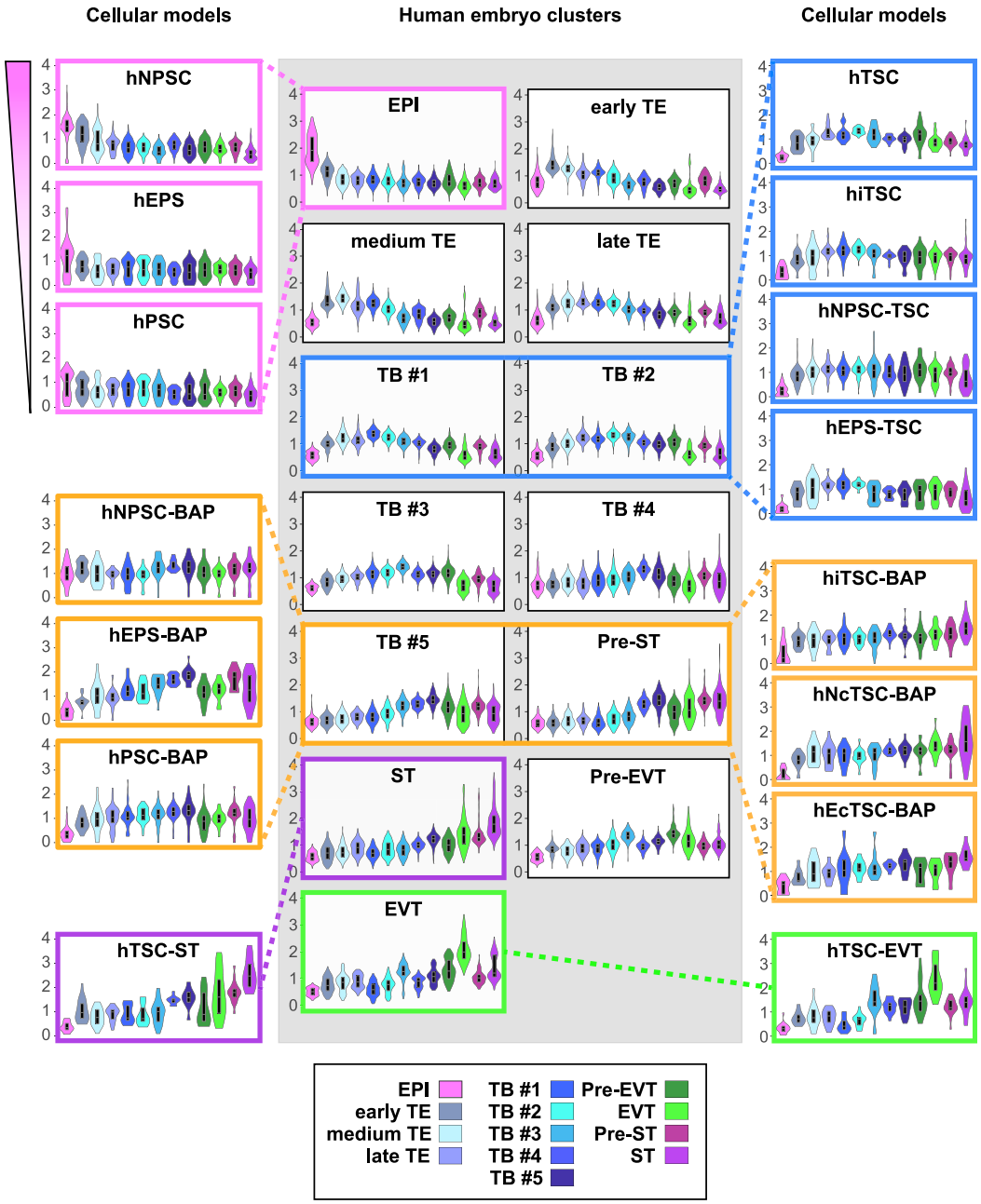

Figure 6. Expression Profiles of Human Embryo Gene Sets in hi/cTSCs

Violin plots summarizing the heatmaps of Figure 5. Gene sets characterizing embryo cell populations are plotted for single-cell clusters (middle, gray-shaded panels) or cellular models for this study (left and right). Within each plot, each violin/boxplot consists of the aggregation of gene sets' expression levels. Expression of each gene is scaled by the standard deviation prior to the aggregation.

SUPPLEMENTAL INFORMATION

Supplemental Information can be found online at https://doi.org/10.1016/j.celrep.2020.108419.

ACKNOWLEDGMENTS

We thank the core facilities GenoBIRD, Micropicell, Cytocell, and iPSCDTC. D.M. is funded by FINOX Forward Initiative. This work was supported by "Paris Scientifique region Pays de la Loire: HUMPLURI."

AUTHOR CONTRIBUTIONS

G.C. and B.B. performed experiments, with the help of other authors. J.B. performed biochemical dosages. D.M., G.C., and S.C. performed bioinformatic analysis, with the help of E.C. G.C. and L.D. conceived the study and wrote the manuscript, with the input of all authors.

DECLARATION OF INTERESTS

D.M. is supported by FINOX forward grant initiative. G.C. and L.D. have a provisional patent filled on the generation of hiTSCs.

Received: August 17, 2019
Revised: August 21, 2020
Accepted: October 29, 2020
Published: November 24, 2020

REFERENCES

Amit, M., Carpenter, M.K., Inokuma, M.S., Chiu, C.-P., Harris, C.P., Waknitz, M.A., Itskovitz-Eldor, J., and Thomson, J.A. (2000). Clonally derived human embryonic stem cell lines maintain pluripotency and proliferative potential for prolonged periods of culture. Dev. Biol. *227*, 271–278.

Amita, M., Adachi, K., Alexenko, A.P., Sinha, S., Schust, D.J., Schulz, L.C., Roberts, R.M., and Ezashi, T. (2013). Complete and unidirectional conversion of human embryonic stem cells to trophoblast by BMP4. Proc. Natl. Acad. Sci. USA *110*, E1212–E1221.

Baker, J.D., Ozsan, I., Rodriguez Ospina, S., Gulick, D., and Blair, L.J. (2018). Hsp90 Heterocomplexes Regulate Steroid Hormone Receptors: From Stress Response to Psychiatric Disease. Int. J. Mol. Sci. *20*, 79.

Bernardo, A.S., Faial, T., Gardner, L., Niakan, K.K., Ortmann, D., Senner, C.E., Callery, E.M., Trotter, M.W., Hemberger, M., Smith, J.C., et al. (2011). BRACHYURY and CDX2 mediate BMP-induced differentiation of human and mouse pluripotent stem cells into embryonic and extraembryonic lineages. Cell Stem Cell *9*, 144–155.

Burton, G.J., Fowden, A.L., and Thornburg, K.L. (2016). Placental Origins of Chronic Disease. Physiol. Rev. *96*, 1509–1565.

Chan, E.M., Ratanasirintrawoot, S., Park, I.H., Manos, P.D., Loh, Y.H., Huo, H., Miller, J.D., Hartung, O., Rho, J., Ince, T.A., et al. (2009). Live cell imaging distinguishes bona fide human iPS cells from partially reprogrammed cells. Nat. Biotechnol. *27*, 1033–1037.

Chng, Z., Teo, A., Pedersen, R.A., and Vallier, L. (2010). SIP1 mediates cell-fate decisions between neuroectoderm and mesendoderm in human pluripotent stem cells. Cell Stem Cell *6*, 59–70.

Cinkornpumin, J.K., Kwon, S.Y., Guo, Y., Hossain, I., Sirois, J., Russett, C.S., Tseng, H.W., Okae, H., Arima, T., Duchaine, T.F., et al. (2020). Naive Human Embryonic Stem Cells Can Give Rise to Cells with a Trophoblast-like Transcriptome and Methylome. Stem Cell Reports *15*, 198–213.

Deglincerti, A., Croft, G.F., Pietila, L.N., Zernicka-Goetz, M., Siggia, E.D., and Brivanlou, A.H. (2016). Self-organization of the in vitro attached human embryo. Nature *533*, 251–254.

Dong, C., Beltcheva, M., Gontarz, P., Zhang, B., Popli, P., Fischer, L.A., Khan, S.A., Park, K.M., Yoon, E.J., Xing, X., et al. (2020). Derivation of trophoblast stem cells from naïve human pluripotent stem cells. eLife *9*, e52504.

El-Hashash, A.H.K., Warburton, D., and Kimber, S.J. (2010). Genes and signals regulating murine trophoblast cell development. Mech. Dev. *127*, 1–20.

Ezashi, T., Schust, D.J., and Schulz, L.C. (2019). Modeling the Placenta with Stem Cells. N. Engl. J. Med. *381*, 1681–1683.

Gao, X., Nowak-Imialek, M., Chen, X., Chen, D., Herrmann, D., Ruan, D., Chen, A.C.H., Eckersley-Maslin, M.A., Ahmad, S., Lee, Y.L., et al. (2019). Establishment of porcine and human expanded potential stem cells. Nat. Cell Biol. *21*, 687–699.

Gerri, C., McCarthy, A., Alanis-Lobato, G., Demtschenko, A., Bruneau, A., Loubersac, S., Fogarty, N.M.E., Hampshire, D., Elder, K., Snell, P., et al. (2020). Initiation of a conserved trophectoderm program in human, cow and mouse embryos. Nature, Published online September 23, 2020. https://doi.org/10.1038/s41586-020-2759-x.

Guo, G., von Meyenn, F., Santos, F., Chen, Y., Reik, W., Bertone, P., Smith, A., and Nichols, J. (2016). Naive Pluripotent Stem Cells Derived Directly from Isolated Cells of the Human Inner Cell Mass. Stem Cell Reports *6*, 437–446.

Guo, G., Stirparo, G.G., Strawbridge, S., Yang, J., Clarke, J., Li, M.A., Myers, S., Özel, B.N., Nichols, J., and Smith, A. (2020). Trophectoderm Potency is Retained Exclusively in Human Naïve Cells. BioRxiv. https://doi.org/10.1101/2020.02.04.933812.

Haghverdi, L., Lun, A.T.L., Morgan, M.D., and Marioni, J.C. (2018). Batch effects in single-cell RNA-sequencing data are corrected by matching mutual nearest neighbors. Nat. Biotechnol. *36*, 421–427.

Haider, S., Meinhardt, G., Saleh, L., Kunihs, V., Gamperl, M., Kaindl, U., Ellinger, A., Burkard, T.R., Fiala, C., Pollheimer, J., et al. (2018). Self-Renewing Trophoblast Organoids Recapitulate the Developmental Program of the Early Human Placenta. Stem Cell Reports *11*, 537–551.

Handschuh, K., Guibourdenche, J., Guesnon, M., Laurendeau, I., Evain-Brion, D., and Fournier, T. (2006). Modulation of PAPP-A expression by PPARgamma in human first trimester trophoblast. Placenta *27* (*Suppl A*), S127–S134.

Home, P., Saha, B., Ray, S., Dutta, D., Gunewardena, S., Yoo, B., Pal, A., Vivian, J.L., Larson, M., Petroff, M., et al. (2012). Altered subcellular localization of transcription factor TEAD4 regulates first mammalian cell lineage commitment. Proc. Natl. Acad. Sci. USA *109*, 7362–7367.

Home, P., Kumar, R.P., Ganguly, A., Saha, B., Milano-Foster, J., Bhattacharya, B., Ray, S., Gunewardena, S., Paul, A., Camper, S.A., et al. (2017). Genetic redundancy of GATA factors in the extraembryonic trophoblast lineage ensures the progression of preimplantation and postimplantation mammalian development. Development *144*, 876–888.

Hunkapiller, N.M., Gasperowicz, M., Kapidzic, M., Plaks, V., Maltepe, E., Kitajewski, J., Cross, J.C., and Fisher, S.J. (2011). A role for Notch signaling in trophoblast endovascular invasion and in the pathogenesis of pre-eclampsia. Development *138*, 2987–2998.

Johnson, W.E., Li, C., and Rabinovic, A. (2007). Adjusting batch effects in microarray expression data using empirical Bayes methods. Biostatistics *8*, 118–127.

Kilens, S., Meistermann, D., Moreno, D., Chariau, C., Gaignerie, A., Reignier, A., Lelièvre, Y., Casanova, M., Vallot, C., Nedellec, S., et al.; Milieu Intérieur Consortium (2018). Parallel derivation of isogenic human primed and naive induced pluripotent stem cells. Nat. Commun. *9*, 360.

Kim, S., Wong, P., and Coulombe, P.A. (2006). A keratin cytoskeletal protein regulates protein synthesis and epithelial cell growth. Nature *441*, 362–365.

Kim, Y., Jeong, J., and Choi, D. (2020). Small-molecule-mediated reprogramming: a silver lining for regenerative medicine. Exp. Mol. Med. *52*, 213–226.

Knöfler, M., Haider, S., Saleh, L., Pollheimer, J., Gamage, T.K.J.B., and James, J. (2019). Human placenta and trophoblast development: key molecular mechanisms and model systems. Cell. Mol. Life Sci. *76*, 3479–3496.

Krendl, C., Shaposhnikov, D., Rishko, V., Ori, C., Ziegenhain, C., Sass, S., Simon, L., Müller, N.S., Straub, T., Brooks, K.E., et al. (2017). GATA2/3-TFAP2A/C transcription factor network couples human pluripotent stem cell differentiation to trophectoderm with repression of pluripotency. Proc. Natl. Acad. Sci. USA *114*, E9579–E9588.

Love, M.I., Huber, W., and Anders, S. (2014). Moderated estimation of fold change and dispersion for RNA-seq data with DESeq2. Genome Biol. *15*, 550.

Lun, A.T., McCarthy, D.J., and Marioni, J.C. (2016). A step-by-step workflow for low-level analysis of single-cell RNA-seq data with Bioconductor. F1000Res. *5*, 2122.

Malassiné, A., Frendo, J.L., and Evain-Brion, D. (2003). A comparison of placental development and endocrine functions between the human and mouse model. Hum. Reprod. Update *9*, 531–539.

Meistermann, D., Loubersac, S., Reigner, A., Firmin, J., Francois Campion, V., Kilens, S., Lelièvre, Y., Lammers, J., Feyeux, M., Hulin, P., et al. (2019). Spatio-temporal analysis of human preimplantation development reveals dynamics of epiblast and trophectoderm. bioRxiv. https://doi.org/10.1101/604751.

Mischler, A., Karakis, V., Mahinthakumar, J., Carberry, C., San Miguel, A., Rager, J., Fry, R., and Rao, B.M. (2019). Two distinct trophectoderm lineage stem cells from human pluripotent stem cells. bioRxiv. https://doi.org/10.1101/762542.

Niakan, K.K., and Eggan, K. (2013). Analysis of human embryos from zygote to blastocyst reveals distinct gene expression patterns relative to the mouse. Dev. Biol. *375*, 54–64.

Nishioka, N., Inoue, K., Adachi, K., Kiyonari, H., Ota, M., Ralston, A., Yabuta, N., Hirahara, S., Stephenson, R.O., Ogonuki, N., et al. (2009). The Hippo signaling pathway components Lats and Yap pattern Tead4 activity to distinguish mouse trophectoderm from inner cell mass. Dev. Cell *16*, 398–410.

Okae, H., Toh, H., Sato, T., Hiura, H., Takahashi, S., Shirane, K., Kabayama, Y., Suyama, M., Sasaki, H., and Arima, T. (2018). Derivation of Human Trophoblast Stem Cells. Cell Stem Cell *22*, 50–63.e56.

Parast, M.M., Yu, H., Ciric, A., Salata, M.W., Davis, V., and Milstone, D.S. (2009). PPARgamma regulates trophoblast proliferation and promotes labyrinthine trilineage differentiation. PLoS ONE *4*, e8055.

Petropoulos, S., Edsgärd, D., Reinius, B., Deng, Q., Panula, S.P., Codeluppi, S., Plaza Reyes, A., Linnarsson, S., Sandberg, R., and Lanner, F. (2016). Single-Cell RNA-Seq Reveals Lineage and X Chromosome Dynamics in Human Preimplantation Embryos. Cell *165*, 1012–1026.

Qiu, X., Mao, Q., Tang, Y., Wang, L., Chawla, R., Pliner, H.A., and Trapnell, C. (2017). Reversed graph embedding resolves complex single-cell trajectories. Nat. Methods *14*, 979–982.

Rayon, T., Menchero, S., Nieto, A., Xenopoulos, P., Crespo, M., Cockburn, K., Cañon, S., Sasaki, H., Hadjantonakis, A.-K., de la Pompa, J.L., et al. (2014). Notch and hippo converge on Cdx2 to specify the trophectoderm lineage in the mouse blastocyst. Dev. Cell *30*, 410–422.

Rivron, N., Pera, M., Rossant, J., Martinez Arias, A., Zernicka-Goetz, M., Fu, J., van den Brink, S., Bredenoord, A., Dondorp, W., de Wert, G., et al. (2018a). Debate ethics of embryo models from stem cells. Nature *564*, 183–185.

Rivron, N.C., Frias-Aldeguer, J., Vrij, E.J., Boisset, J.-C., Korving, J., Vivié, J., Truckenmüller, R.K., van Oudenaarden, A., van Blitterswijk, C.A., and Geijsen, N. (2018b). Blastocyst-like structures generated solely from stem cells. Nature *557*, 106–111.

Saha, B., Ganguly, A., Home, P., Bhattacharya, B., Ray, S., Ghosh, A., Rumi, M.A.K., Marsh, C., French, V.A., Gunewardena, S., and Paul, S. (2020). TEAD4 ensures postimplantation development by promoting trophoblast self-renewal: An implication in early human pregnancy loss. Proc. Natl. Acad. Sci. USA *117*, 17864–17875.

Schaiff, W.T., Carlson, M.G., Smith, S.D., Levy, R., Nelson, D.M., and Sadovsky, Y. (2000). Peroxisome proliferator-activated receptor-γ modulates differentiation of human trophoblast in a ligand-specific manner. J. Clin. Endocrinol. Metab. *85*, 3874–3881.

Soumillon, M., Cacchiarelli, D., Semrau, S., van Oudenaarden, A., and Mikkelsen, T.S. (2014). Characterization of directed differentiation by high-throughput single-cell RNA-Seq. bioRxiv. https://doi.org/10.1101/003236.

Takahashi, K., Tanabe, K., Ohnuki, M., Narita, M., Ichisaka, T., Tomoda, K., and Yamanaka, S. (2007). Induction of pluripotent stem cells from adult human fibroblasts by defined factors. Cell *131*, 861–872.

Takashima, Y., Guo, G., Loos, R., Nichols, J., Ficz, G., Krueger, F., Oxley, D., Santos, F., Clarke, J., Mansfield, W., et al. (2014). Resetting transcription factor control circuitry toward ground-state pluripotency in human. Cell *158*, 1254–1269.

Thomson, J.A., Itskovitz-Eldor, J., Shapiro, S.S., Waknitz, M.A., Swiergiel, J.J., Marshall, V.S., and Jones, J.M. (1998). Embryonic stem cell lines derived from human blastocysts. Science *282*, 1145–1147.

Turco, M.Y., and Moffett, A. (2019). Development of the human placenta. Development *146*, dev163428.

Turco, M.Y., Gardner, L., Kay, R.G., Hamilton, R.S., Prater, M., Hollinshead, M.S., McWhinnie, A., Esposito, L., Fernando, R., Skelton, H., et al. (2018). Trophoblast organoids as a model for maternal-fetal interactions during human placentation. Nature *564*, 263–267.

Wakeland, A.K., Soncin, F., Moretto-Zita, M., Chang, C.W., Horii, M., Pizzo, D., Nelson, K.K., Laurent, L.C., and Parast, M.M. (2017). Hypoxia Directs Human Extravillous Trophoblast Differentiation in a Hypoxia-Inducible Factor-Dependent Manner. Am. J. Pathol. *187*, 767–780.

Xiang, L., Yin, Y., Zheng, Y., Ma, Y., Li, Y., Zhao, Z., Guo, J., Ai, Z., Niu, Y., Duan, K., et al. (2020). A developmental landscape of 3D-cultured human pre-gastrulation embryos. Nature *577*, 537–542.

Yang, Y., Liu, B., Xu, J., Wang, J., Wu, J., Shi, C., Xu, Y., Dong, J., Wang, C., Lai, W., et al. (2017). Derivation of Pluripotent Stem Cells with In Vivo Embryonic and Extraembryonic Potency. Cell *169*, 243–257.e25.

Zhou, F., Wang, R., Yuan, P., Ren, Y., Mao, Y., Li, R., Lian, Y., Li, J., Wen, L., Yan, L., et al. (2019). Reconstituting the transcriptome and DNA methylome landscapes of human implantation. Nature *572*, 660–664.

STAR★METHODS

KEY RESOURCES TABLE

REAGENT or RESOURCE	SOURCE	IDENTIFIER
Antibodies		
GATA2	Sigma-Aldrich	WH0002624M1; RRID:AB_1841726
GATA3	R&D	AF2605; RRID:AB_2108571
NR2F2	Abcam	ab211776
CGB	Abcam	ab9582; RRID:AB_296507
HLA-G	Abcam	ab52455; RRID:AB_880552
DSP	Abcam	ab71690; RRID:AB_1603776
SOX2	SCBT	sc-17320; RRID:AB_2286684
Donkey anti-rabbit-Alexa Fluor 488	ThermoFisher	A21206; RRID:AB_2535792
Donkey anti-mouse-Alexa Fluor 568	ThermoFisher	A10037; RRID:AB_2534013
Donkey anti-goat-Alexa Fluor 647	ThermoFisher	A21447; RRID:AB_141844
Biological Samples		
Villous cytotrophoblasts from 1st trimester human placenta	Thierry Fournier's lab	1536
Villous cytotrophoblasts from 1st trimester human placenta	Thierry Fournier's lab	1560
Extravillous trophoblasts from 1st trimester human placenta	Thierry Fournier's lab	1478
Extravillous trophoblasts from 1st trimester human placenta	Thierry Fournier's lab	1657
Chemicals, Peptides, and Recombinant Proteins		
Y27632 (ROCK inhibitor)	Axon Medchem	1683
Insulin-Transferrin-Selenium-Ethanolamine supplement (ITS-X)	GIBCO	51500-056
L-ascorbic acid	Sigma-Aldrich	A7506
hEGF	Miltenyi Biotec	130-097-751
CHIR99021	Axon Medchem	1386
A83-01	Axon Medchem	1421
SB431542	Axon Medchem	1661
valproic acid	Sigma-Aldrich	P4543
PD0325901	Axon Medchem	1408
mLIF	Miltenyi Biotec	130-095-779
Gö6983	Axon Medchem	2466
N2 supplement	GIBCO	17502048
B27 supplement	GIBCO	17504-001
B27 supplement minus vitamin A	GIBCO	12587010
human LIF	Miltenyi Biotec	130-108-156
(S)-(+)-Dimethindene maleate	Tocris	1425
Minocycline hydrochloride	Tocris	3268
IWR-endo-1	Axon Medchem	2510
human fibroblast growth factor 2	Peprotech	100-18B
human NRG1	CST	5218SC
Forskolin	Axon Medchem	2264
human R-Spondin-1	Peprotech	120-38
human HGF	Peprotech	100-39H

(*Continued on next page*)

Continued

REAGENT or RESOURCE	SOURCE	IDENTIFIER
N-Acetyl-L-cysteine	Sigma-Aldrich	A9165
Bovine Serum Albumin (BSA)	Sigma-Aldrich	A3059
Mitomycin C	Sigma-Aldrich	M4287
Critical Commercial Assays		
Elecsys free βhCG	Cobas/Roche	04854071
Deposited Data		
DGE-seq datasets generated by this study	This paper; ENA	https://www.ebi.ac.uk/ena/browser/view/PRJEB34037
Code generated by this study	This paper; GitLab	https://gitlab.univ-nantes.fr/E137833T/Castel_et_al_2020
Experimental Models: Cell Lines		
CT30	Okae et al., 2018; Riken BioBank	RCB4938
CT1	Okae et al., 2018	N/A
CT2	Okae et al., 2018	N/A
BL1	Okae et al., 2018	N/A
BL2	Okae et al., 2018	N/A
AV01	This paper	N/A
AV02	This paper	N/A
AV03	This paper	N/A
AV04	This paper	N/A
AV11	This paper	N/A
AV12	This paper	N/A
AV21	This paper	N/A
AV22	This paper	N/A
AV23	This paper	N/A
AV24	This paper	N/A
L8A2	Kilens et al., 2018	N/A
M2A8	Kilens et al., 2018	N/A
M8A9	Kilens et al., 2018	N/A
M8A15	Kilens et al., 2018	N/A
M2A18	Kilens et al., 2018	N/A
HNES1	Guo et al., 2016	N/A
EPS01	This paper	N/A
EPS02	This paper	N/A
H9 (WA09)	Thomson et al., 1998	N/A
L8K1	Kilens et al., 2018	N/A
L8B1	Kilens et al., 2018	N/A
Oligonucleotides		
Primer: CGA Forward: CAGAATGCACGCTACAGGAA	Eurofins Genomics	N/A
Primer: CGA Reverse: CGTGTGGTTCTCCACTTTGA	Eurofins Genomics	N/A
Primer: CGB Forward: TGTGCATCACCGTCAACA	Eurofins Genomics	N/A
Primer: CGB Reverse: TGCACATTGACAGCTGAGAG	Eurofins Genomics	N/A
Primer: SDC1 Forward: GGATGACTCTGACAACTTCTCC	Eurofins Genomics	N/A

(*Continued on next page*)

Continued

REAGENT or RESOURCE	SOURCE	IDENTIFIER
Primer: SDC1 Reverse: CTACAGCCTCTCCCTCCTT	Eurofins Genomics	N/A
Primer: HLA-G Forward: GCCAATGTGGCTGAACAAAG	Eurofins Genomics	N/A
Primer: HLA-G Reverse: TATGATCTCCGCAGGGTAGAA	Eurofins Genomics	N/A
Primer: MMP2 Forward: GGCACCCATTTACACCTACA	Eurofins Genomics	N/A
Primer: MMP2 Reverse: AACCGGTCCTTGAAGAAGAAG	Eurofins Genomics	N/A
The full list of primers used in this study can be found in Table S1B	N/A	N/A
Software and Algorithms		
Volocity	Quorum technologies	v6.5
Fiji	ImageJ	v1.52p
StepOne	Thermofisher	v2.3
R	Bioconductor	v4.0
Other		
scRNA-seq dataset from Petropoulos et al.	Petropoulos et al., 2016; ArrayExpress	https://www.ebi.ac.uk/arrayexpress/experiments/E-MTAB-3929/
scRNA-seq dataset from Zhou et al.	Zhou et al., 2019; GEO	https://www.ncbi.nlm.nih.gov/geo/query/acc.cgi?acc=GSE109555
scRNA-seq dataset from Xiang et al.	Xiang et al., 2020; GEO	https://www.ncbi.nlm.nih.gov/geo/query/acc.cgi?acc=GSE136447

RESOURCE AVAILABILITY

Lead Contact

Further information and requests for resources and reagents should be directed to and will be fulfilled by the Lead Contact, Dr Laurent DAVID (laurent.david@univ-nantes.fr)

Materials Availability

There are restrictions to the availability of cell lines due to the lack of an external centralized repository for their distribution and our need to maintain the stock. We are glad to share cell lines with reasonable compensation by requestor for their processing and shipping. We may require a completed Materials Transfer Agreement if there is potential for commercial application.

Data and Code Availability

The datasets generated during this study (DGE-seq) are available at European Nucleotide Archive (ENA) https://www.ebi.ac.uk/ena/browser/view/PRJEB34037. The code generated during this study is available at GitLab https://gitlab.univ-nantes.fr/E137833T/Castel_et_al_2020.

The scRNA-seq dataset from Petropoulos et al. (2016) is available at ArrayExpress https://www.ebi.ac.uk/arrayexpress/experiments/E-MTAB-3929/. The scRNA-seq dataset from Zhou et al. (2019) is available at NCBI Gene Expression Omnibus (GEO) https://www.ncbi.nlm.nih.gov/geo/query/acc.cgi?acc=GSE109555. The scRNA-seq dataset from Xiang et al. (2020) is available at NCBI Gene Expression Omnibus (GEO) https://www.ncbi.nlm.nih.gov/geo/query/acc.cgi?acc=GSE136447.

EXPERIMENTAL MODEL AND SUBJECT DETAILS

Cell lines

For human somatic cell reprogramming into hiTSCs and hiEPSs, fibroblasts from healthy donors were used: BJ1, male fibroblasts are commercial BJ human neonatal fibroblasts extracted from normal human foreskin (Stemgent Cat# 08-0027); L71 from a 51-year-old healthy man; L80 from a 57-year-old healthy woman. Those fibroblasts were previously used to generate isogenic hiPSCs and hiNPSCs (Kilens et al., 2018). For conversion experiments, we used hiNPSC and hiPSC lines from Kilens et al., and H9 hESCs

(WA09 Lot WB0090) obtained from the WiCell Research Institute. hESCs were used under authorization RE17-007R from the French oversight committee, Agence de la Biomédecine. All cell lines used in this study are further described in Table S1A.

Human preimplantation embryos

Data analysis and transcriptomic modeling of human preimplantation development is detailed in Meistermann et al. (2019).

METHOD DETAILS

Experimental design

Biological replicates are indicated in each figure. Randomization and blinding were performed for qRT-PCR but not for other experiments. No data or samples were excluded from any of the experiments.

Tissue culture

All cell lines were cultured at 37 °C, under hypoxic (5% O_2, 5% CO_2) or normoxic conditions (20% O_2, 5% CO_2) as indicated. Culture medium was daily replaced. 10 μM Y27632 (Axon Medchem) was added to the culture medium upon cell seeding of human stem cells. PXX indicates passage number, and P+XX indicates that cells were converted for XX passages.

Human fibroblasts were cultured in fibroblast medium, composed of high glucose Dulbecco's modified Eagle's medium (DMEM) GlutaMAX-I (GIBCO) supplemented with 10% fetal bovine serum (FBS, Hyclone), 1% sodium pyruvate (GIBCO) and 1% non-essential amino acids (GIBCO).

Mouse embryonic fibroblasts (MEFs) were prepared from E13.5 pups that were decapitated, eviscerated, dissociated with 0.25% trypsin, 0.1% EDTA and plated in MEF medium [DMEM high glucose (Thermo Scientific ®), Glutamax 1:100 (GIBCO®), 0.5% of penicillin–streptomycin (Life Technologies)] on 0.1% gelatin-coated plates. MEFs were mitotically inactivated using 0.01mg/ml mitomycin C (Sigma-Aldrich®) to be used as feeder cells. MEF isolation was performed in compliance with the French law and under supervision of the UTE animal core facility, University of Nantes.

hiTSCs were cultured on MEF feeder cells in hTSC medium (Okae et al., 2018) [DMEM/F12 (GIBCO) supplemented with 0.1mM 2-mercaptoethanol (GIBCO), 0.2% FBS, 0.5% penicillin-streptomycin, 0.3% Bovine Serum Albumin (BSA, Sigma-Aldrich), 1% Insulin-Transferrin-Selenium-Ethanolamine supplement (ITS-X, GIBCO), 1.5 mg/ml L-ascorbic acid (Sigma-Aldrich), 50 ng/ml hEGF (Miltenyi Biotec), 2 μM CHIR99021 (Axon Medchem), 0.5 μM A83-01 (Tocris), 1 μM SB431542 (Tocris), 0.8 mM valproic acid (Sigma-Aldrich) and 5 μM Y27632]. hiTSCs could be passaged with TrypLE (15 min, 37°C, Life Technologies) every 4 days at a 1:3 to 1:4 split ratio or every 7 days at a 1:40 to 1:60 split ratio. hiTSCs were routinely cultured at 37°C in hypoxic conditions (5% O_2, 5% CO_2).

hNPSCs were cultured on MEF feeder cells in t2iLGöY medium (Takashima et al., 2014) [DMEM/F12 supplemented with 1% N2 (GIBCO), 1% B27 (GIBCO), 1% non-essential amino acids, 1% GlutaMAX (GIBCO), 0.1 mM 2-mercaptoethanol, 50 μg/ml BSA, 0.5% penicillin–streptomycin, 1 μM CHIR99021, 1 μM PD0325901 (Axon Medchem), 20 ng/ml mLIF (Miltenyi Biotec), 5 μM Gö6983 (Axon Medchem) and 10 μM Y27632] (Takashima et al., 2014). hNPSCs were passaged every 4 days at a 1:3 split ratio using TrypLE (5 min, 37°C, Life Technologies). hNPSCs were routinely cultured at 37 °C in hypoxic conditions (5% O_2, 5% CO_2).

hEPSs were cultured on MEF feeder cells in LCDM medium (Yang et al., 2017) [48% DMEM/F12 and 48% Neurobasal (GIBCO) supplemented with 0.5% N2 supplement, 1% B27 supplement minus vitamin A (GIBCO), 1% non-essential amino acids, 0.1 mM 2-mercaptoethanol, 0.5% penicillin-streptomycin, 5% knockout serum replacement (KSR, GIBCO), 10 ng/ml human LIF (Miltenyi Biotec), 1μM CHIR99021, 2 μM (S)-(+)-Dimethindene maleate (Tocris) and 2 μM Minocycline hydrochloride (Tocris), 1 μM IWR-endo-1 (Miltenyi Biotec) and 2 μM Y-27632] (Yang et al., 2017). hEPSs were passaged every 4 days at a 1:8 split ratio using TrypLE (5 min, 37°C, Life Technologies). hEPSs were routinely cultured at 37°C in normoxic conditions (20% O_2, 5% CO_2).

Primed hPSCs could be cultured on MEF feeder cells in KSR+FGF2 medium (Amit et al., 2000) [DMEM/F12 supplemented with 20% KSR, 1% non-essential amino acids, 1% GlutaMAX, 50 μM 2-mercaptoethanol, 0.5% penicillin-streptomycin and 10 ng/ml human fibroblast growth factor 2 (FGF2, Peprotech)]. 10 colonies were manually picked every 7 days for passage and seeded as small clumps (~200 μm) in a new 35mm dish. Primed hPSCs could also be cultured on MEF feeder cells in iPS-Brew medium (Miltenyi Biotec) and these cells were passaged every 4 to 6 days at a 1:8 to 1:25 split ratio using TrypLE (5 min, 37°C, Life Technologies). Primed hPSCs were routinely cultured at 37°C in normoxic conditions (20% O_2, 5% CO_2).

10μM ROCK inhibitor (Y-27632) was systematically added to the culture media for 1 day after cell passaging with TrypLE. All cell lines were tested negative for mycoplasma using the MycoAlert kit (LONZA, LT07-318).

Somatic cell reprogramming to hiTSC

Human adult fibroblasts were reprogrammed using the CytoTune-iPS 2.0 Sendai reprogramming kit (Life Technologies). Two days before infection, 3.0 to 4.0 × 10^4 fibroblasts were seeded per well on a 12-well plate, coated with Matrigel. At day 0, cells were infected with the three vectors: polycistronic Klf4-Oct4-Sox2, Myc and Klf4 at a 5:5:3 or 3:3:3 multiplicity of infection (MOI) respectively. At day 9 of infection, cells were dissociated with TrypLE (5 min, 37°C, Life Technologies) and seeded in 35mm dishes, on MEFs. On the following day, cells were transited into E7 reprogramming medium (STEMCELL Technologies). From day 21 onward, cells were transited into hTSC medium. Induced hTSC lines (hiTSC) were routinely cultured at 37°C in hypoxic conditions (5% O_2, 5%CO_2).

Somatic cell reprogramming to hiNPSCs, hiEPSs and hiPSCs was performed as described in previous reports (Kilens et al., 2018; Yang et al., 2017).

Conversion of hNPSC and hEPS to hcTSC

hNPSCs and hEPSs were dissociated with TrypLE (5 min, 37°C, Life Technologies) and seeded in 35mm dishes, on MEFs, at a density of 0.6 to 1.7 × 10^5 cells per dish. Cells were maintained in their initial medium supplemented with 10 μM Y27632 for 1 day. From day 2 onward, cells were transited into hTSC medium. Converted hTSC lines (hcTSC) were routinely cultured at 37°C in hypoxic conditions (5% O_2, 5% CO_2).

Primed hPSCs included in conversion experiments were initially cultured in KSR+FGF2 or iPS-BREW. 10 colonies were picked (KSR+FGF2) or cells were passaged with TrypLE (iPS-BREW) and seeded at a density of 0.5 to 1.25 × 10^5 cells per dish in 35mm dishes coated with MEFs for conversion assays.

Differentiation of hi/cTSC to EVT and ST

After at least 15 passages, cells were collected for differentiation assays.

Prior to differentiation into ST and EVT cells, h(i/c)TSCs (initially cultured on MEFs) were transited to fibronectin for at least 3 passages.

EVT differentiation

2-4 days before passage, h(i/c)TSCs were transited into pre-EVT medium [DMEM/F12 supplemented with 0.1mM 2-mercaptoethanol, 0.5% penicillin-streptomycin, 0.3% BSA, 1% ITS-X supplement, 4% KSR, 7.5 μM A83-01 (Tocris), 2.5 μM Y27632, 5 μM IWR-endo-1 (Miltenyi Biotec)]. Then, cells were passaged with TrypLE to a density of 0.8 to 3.0 × 10^4 cells/cm^2. Before treatment was initiated, cells were placed in differentiation basal medium [DMEM/F12 containing 0.1 mM 2-mercaptoethanol, 0.5% Penicillin-Streptomycin, 0.3% BSA, 1% ITS-X], supplemented with 10 μM ROCK inhibitor (Y27632). Within 6 hours, timing depending on the lines, cells were transited into EVT medium (Okae et al., 2018) [Differentiation basal medium, supplemented with 100 ng/ml NRG1, 7.5 mM A83-01, 2.5 mM Y27632, 4% KnockOut Serum Replacement, 2% Matrigel]. At day 3, medium was replaced with the EVT medium containing 0.5% Matrigel, without NRG1. Typically, EVT formation was observed by day 4-5. At day 6, medium was replaced with the EVT medium containing 0.5% Matrigel, without NRG1 and KSR. Cells were collected on day 8 for subsequent analyses.

2D-ST differentiation

h(i/c)TSCs were passaged with TrypLE to a density of 2.0 to 6.0 × 10^4 cells/cm^2. Before treatment was initiated, cells were placed in differentiation basal medium [DMEM/F12 containing 0.1 mM 2-mercaptoethanol, 0.5% Penicillin-Streptomycin, 0.3% BSA, 1% ITS-X], supplemented with 10 μM ROCK inhibitor (Y27632). Within 3 hours, timing depending on the lines, cells were transited into ST medium (Okae et al., 2018) [Differentiation basal medium, supplemented with 2.5 mM Y27632, 2 mM forskolin, and 4% KSR]. Medium was replaced at day 3, and cells were analyzed at day 6.

3D-ST differentiation

Prior to 3D differentiation assay, h(i/c)TSCs were transited to trophoblast organoid medium (TOM) with small modifications (Turco et al., 2018) [DMEM/F12, 1X N2 supplement, 1X B27 supplement minus vitamin A, 1.25 mM N-Acetyl-L-cysteine, 1% GlutaMAX (GIBCO), 0.5% Penicillin-Streptomycin (TOM basal medium), supplemented with 500 nM A83-01, 1.5 μM CHIR99021, 80 ng/ml human R-spondin1, 50 ng/ml hEGF, 100 ng/ml hFGF2, 50 ng/ml hHGF, 2 μM Y-27632]. 0.4 to 1.0 × 10^5 cells passaged with TrypLE were embedded into 150μl drops comprising: 50μl Matrigel and 50μl PBS+/+ along with 960 ng fibronectin, 50 ng laminin521 and 50μl TOM basal medium. Drops were carefully deposited on sterile parafilm covered dishes and placed at 37°C for 20 minutes to solidify. Complete TOM supplemented with 10 μM ROCK inhibitor (Y27632) was further added to cover the drops. Medium was replaced every 3 days with TOM. The 3D structures emerged within a week and were collected on day14 for subsequent analyses.

MEF-BAP treatment

hPSC and hi/cTSC lines were dissociated with TrypLE and seeded on 35mm dishes coated with MEFs, at a density of 0.4 to 1.0 × 10^5 cells per dish. For primed hPSCs cultured in KSR +FGF2 medium, about 10 colonies were manually picked and seeded per dish. hPSCs and hi/cTSCs were maintained in their initial medium supplemented with 10 μM Y27632 for 1 day. The following day, initial medium was replaced with MEF-BAP (Amita et al., 2013) [DMEM/F12 supplemented with 20% KSR, 1% non-essential amino acids, 1% GlutaMAX, 50μM 2-mercaptoethanol (MEF-CM, conditioned for 24 hours on a MEF monolayer and filtrated with a 0.22 μm pore size filtration unit), 2 ng/ml human BMP4 (Miltenyi Biotec), 1μM A83-01 and 0.1 μM PD173074 (Axon Medchem)]. MEF-BAP medium was daily replaced. Supernatants and cells were collected at day 3 and 6 of differentiation for subsequent analyses.

Isolation of VCT, ST and EVT cells from human placentas

Isolation of placental cell types was conducted following previously published protocols (Handschuh et al., 2006). Briefly, chorionic villi were dissected from term placentas of healthy mothers. Mononucleated cytotrophoblasts (VCTs) and extravillous trophoblasts (EVTs) were isolated after trypsin-DNase digestion, sedimentation, filtration and discontinuous Percoll gradient fractionation. VCTs

were cultured for 2h in Dulbecco's modified Eagle's medium (DMEM) containing 10% decomplemented fetal calf serum (FCS), 2 mM glutamine, 100 IU/mL penicillin and 100 mg/mL streptomycin. EVTs were cultured on Matrigel in the same culture conditions for 48h. ST cells were obtained by further differentiation of VCTs for 72h in these conditions (spontaneous aggregation and fusion of VCTs).

β-hCG dosage

Cell culture supernatants were collected at days 0, 3 and 6 of forskolin and MEF-BAP treatments. Amounts of secreted β-hCG were measured by electrochemiluminescence immunoassay "ECLIA" (Elecsys free βhCG, Cobas/Roche®) on Cobas® e601 immunoassay analyzer, at the Clinical Biochemistry Laboratory, CHU Nantes, France.

Immunostaining

For immunofluorescence (IF) analysis, cells were fixed at room temperature using 4% paraformaldehyde for 15 min. Samples were then permeabilized for 60 min at room temperature with IF buffer [phosphate-buffered saline (PBS), 0.2% Triton, 10% FBS], which also served as a blocking solution. Samples were incubated with primary antibodies overnight at 4 °C. The following antibodies were used: anti-GATA2 (1:50 ; Sigma® WH0002624M1), anti-GATA3 (1:100, R&D® AF2605), anti-NR2F2 (1:100, Abcam® ab211776), anti-CGB (1:100, Abcam® ab9582), anti-HLA-G (1:100, Abcam® 52455), anti-DSP (1:200, ref: Abcam® ab71690), anti-SOX2 (1:500, SCBT® sc-17320). Incubation with secondary antibodies was performed for 2 h at room temperature along with 4′,6-diamidino-2-phenylindole (DAPI) nuclei staining. Confocal immunofluorescence images were acquired with A1-SIM Nikon® confocal microscope. Optical sections of 0.5-1 μm-thick were collected. Images were processed using Volocity® visualization software.

RNA extraction and qRT-PCR

Total RNA was extracted using RNeasy® columns and DNase-treated using RNase-free DNase (QIAGEN®). First-strand cDNAs were generated using 500ng of RNA, M-MLV reverse transcriptase (Life technologies®), 25μg/ml polydT (Ambion®) and 9.6μg/ml random primers (Roche®).

qRT-PCR were performed on a StepOne instrument (Applied Biosystems®) using power SYBR green PCR master mix, for genes listed in the primers table (Table S1B). For each sample, the ratio of specific mRNA level relative to *GAPDH* levels was calculated. Experimental results are shown as relative gene expression.

DGE-Seq data generation

For 3′ DGE profiling, RNA-sequencing protocol was performed according to our implementation of Soumillon et al. protocol (Kilens et al., 2018; Soumillon et al., 2014). Briefly, the libraries were prepared from 10 ng of total RNA. The mRNA poly(A) tails were tagged with universal adapters, well-specific barcodes and unique molecular identifiers (UMIs) during template-switching reverse transcription. Barcoded cDNAs from multiple samples were then pooled, amplified and tagmented using a transposon-fragmentation approach which enriches for 3′ends of cDNAs. A library of 350–800 bp was run on an Illumina® HiSeq 2500 using a Hiseq Rapid SBS Kit v2-50 cycles and a Hiseq Rapid PE Cluster Kit v2.

QUANTIFICATION AND STATISTICAL ANALYSIS

DGE-Seq data preprocessing

Read pairs used for analysis matched the following criteria: all 16 bases of the first read had quality scores of at least 10 and the first 6 bases correspond exactly to a designed well-specific barcode. The second reads were aligned to RefSeq human mRNA sequences (hg19) using bwa version 0.7.17. Reads mapping to several transcripts of different genes or containing more than 3 mismatches with the reference sequences were filtered out from the analysis. DGE profiles were generated by counting for each sample the number of unique UMIs associated with each RefSeq genes. DGE-sequenced samples were acquired from five sequencing runs. Sequenced samples with at least 50000 counts and 6000 expressed genes were retained for further analysis.

Transcriptomic analyses from DGE-Seq data

Samples were filtered out if the number of unique UMIs was inferior to 50000 and the number of expressed genes inferior to 6000; 165 samples passed those cutoffs. Samples were normalized using same strategy as described in the DESeq2 method (Love et al., 2014). For performing dimension reduction and clustering, samples were logged using a log2(x+1) transformation. The five different runs were merged using ComBat (Johnson et al., 2007) from the library "sva" in parametric mode, using technical replicates between batches as references for computing batch effects. Each gene expression of the corrected values was subtracted by the minimum of the gene expression before the batch correction. This step does not change the relative expression of genes; however, it permits an easier interpretation of the expression values as minimums cannot be less than zero. Finally, each set of technical replicates were merged. The resulting samples consist in the median of each gene for its set of technical replicates. A set of over-dispersed genes was determined for computing the correlation heatmap from Figure 1C and the PCA from Figures 3 and S1C. To pick these, the coefficient of variation of each gene from the normalized adjusted expression was fitted by the mean expression of each gene, using a LOESS method. Genes with a positive residual for the regression were marked as over-dispersed. This leads to a total of 2770 genes. Pathway eigengenes and their gene contribution were computed with the following steps: first, the gene sets corresponding to each

pathway were downloaded on the KEGG database. Pathways with at least 4 genes existing in our data were conserved. Second, a PCA was computed for each pathway, using the gene set of the pathway as the input of the PCA. The first component of each PCA was designated as "pathway eigengene." In heatmaps, unless otherwise stated, samples are clustered from the Euclidean distance of expression, by a hierarchical clustering using Ward's method. Genes are clustered from a co-expression distance (distance of biweight midcorrelation) between gene expressions, by a hierarchical clustering using Ward's method.

Transcriptomic analyses from single-cell RNA-Seq data

Datasets (Petropoulos et al., 2016; Zhou et al., 2019) were normalized and log transformed using scran (Lun et al., 2016), then merged with *fastMNN* from the R library "batchelor" (Haghverdi et al., 2018) with the parameter *k* set up to 420. UMAP was performed on all available genes with the R library "uwot." The n_neighbors parameter was set to its maximum (6838), and min_dist = 0.2. A first cell clustering was done using Monocle3 (Qiu et al., 2017), then, preimplantation clusters were re-annotated using clusters found in Meistermann et al. (2019). First, coordinates of centroids of these previous clusters were determined on the UMAP using Petropoulos dataset, then, cells were attributed to the cluster with the nearest centroid in term of Euclidean distance. To determine the markers of each clusters, genes with at least a mean 2 normalized count in DGE-Seq and 4 normalized count in single-cell RNA-Seq were kept for computing AUROCs. Genes with an AUC of at least 0.85 were designated as markers. Markers determined by Xiang et al. (2020) were also filtered, with a mean expression of at least 2 normalized counts in DGE-Seq data.

Statistical tests and group size

Data were processed using R. All statistical tests are indicated in the figure legends. Group size (n) is represented by dots projected on boxplots (Figures 1D, 2C, S1D, S2B, and S2C), vertically aligned dots in scatterplots (Figure S3D), vertical slices on heatmaps (Figures 1C, 5 [right], S4–S6 [right]), or specific shaped and colored dots projected on PCA (Figures 3A–3G and S1C) which correspond to biological replicates. For marker gene expression levels, significance ($p < 0.05$) between two groups was calculated using the unpaired two-samples Wilcoxon-Mann-Whitney test that was computed with the stat_compare_means() function from ggplot2 R package. The Wilcoxon-Mann-Whitney test was chosen for stringency, low propensity to produce false positive results and for well-fitting the data. Given our type of data, no specific method was used to determine whether the data met assumptions of the statistical approach.